MOLECULAR AND CELLULAR BIOLOGY, June 2009, p. 3045–3061 Vol. 29, No. 11
0270-7306/09/$08.00+0 doi:10.1128/MCB.00011-09

The Protocadherin Gene *Celsr3* Is Required for Interneuron Migration in the Mouse Forebrain▽

Guoxin Ying,[1] Sen Wu,[2] Ruiqing Hou,[3] Wei Huang,[1] Mario R. Capecchi,[1,2] and Qiang Wu[1,3]*

Department of Human Genetics, University of Utah, Salt Lake City, Utah 84112[1]; Howard Hughes Medical Institute, University of Utah, Salt Lake City, Utah 84112[2]; and Shanghai Center for Systems Biomedicine, Key Laboratory of Systems Biomedicine (Ministry of Education), Shanghai Jiao Tong University, Shanghai 200240, China[3]

Received 5 January 2009/Returned for modification 2 March 2009/Accepted 20 March 2009

Interneurons are extremely diverse in the mammalian brain and provide an essential balance for functional neural circuitry. The vast majority of murine cortical interneurons are generated in the subpallium and migrate tangentially over a long distance to acquire their final positions. By using a mouse line with a deletion of the *Celsr3* (*Flamingo*, or *Fmi1*) gene and a knock-in of the green fluorescent protein reporter, we find that *Celsr3*, a member of the nonclustered protocadherin (*Pcdh*) family, is predominantly expressed in the cortical interneurons in adults and in the interneuron germinal zones in embryos. We show that *Celsr3* is crucial for interneuron migration in the developing mouse forebrain. Specifically, in *Celsr3* knockout mice, calretinin-positive interneurons are reduced in the developing neocortex, accumulated in the corticostriatal boundary, and increased in the striatum. Moreover, the laminar distribution of cortical calbindin-positive cells is altered. Finally, we found that expression patterns of *NRG1* (neuregulin-1) and its receptor *ErbB4*, which are essential for interneuron migration, are changed in *Celsr3* mutants. These results demonstrate that the protocadherin *Celsr3* gene is essential for both tangential and radial interneuron migrations in a class-specific manner.

Cadherins are a superfamily of calcium-binding cell adhesion glycoproteins that are crucial for embryonic neural morphogenesis and adult neuronal connectivity (21, 42). Members of the cadherin (*cdh*) family have been shown to play important roles in neural development and function, such as neurulation, dendritic morphogenesis, axon pathfinding, and synaptic target recognition and plasticity (6). Based on the neural functions and genomic mapping of cadherins, a cadherin hypothesis for neuropsychiatric diseases has been proposed (64). The mammalian cadherin superfamily contains more than 100 diverse members that include classic cadherins, desmosomal cadherins, and protocadherins (*Pcdh*). The *Pcdh* genes constitute the largest subfamily of cadherins and include about 60 clustered and 20 nonclustered genes (21, 61).

The mammalian cadherin, EGF LAG seven-pass G-type receptors 1 to 3 (*Celsr1-3*) are an unusual class of nonclustered *Pcdh* genes (15, 20, 38, 48, 60). The molecular structures of the encoded CELSR proteins are unique in that they contain seven transmembrane domains characteristic of secretin receptor-type G-protein-coupled receptors. In addition, their extracellular domains contain nine cadherin ectodomains, and several EGF as well as laminin A-G motifs (Fig. 1A) (20, 60). These mammalian *Celsr* genes are homologs of the *Drosophila* protocadherin *Flamingo* (*Fmi*) gene which functions in three distinct developmental pathways, including planar cell polarity (PCP) (51), dendritic field maturation (18), and axonal development (51). These functions are thought to be accomplished by mammalian *Celsr1* (*Fmi2*), *Celsr2*, and *Celsr3* (*Fmi1*), respectively (47). First, inactivation of *Celsr1* in mice impairs the characteristic planar arrangements of hair cells in the inner ear (11). In addition, the zebrafish *Celsr1* mediates polarized rearrangements during convergence and extension of gastrulation, a process related to PCP (16). Second, RNA interference knockdown of *Celsr2* results in dendritic simplification in vitro (40). Finally, *Celsr3* has recently been shown to be crucial for axonal tract development in mice (47, 65).

Here, we report a novel function of *Pcdh Celsr3* in interneuron migration in the developing mouse forebrain. Using a new mouse gene-targeting allele of *Celsr3* knockout with an enhanced green fluorescent protein (eGFP) reporter, we first found that *Celsr3* is prominently expressed in the interneuron germinal zones of the ventral telencephalon and in the postnatal and adult cortical GABAergic (where GABA is γ-aminobutyric acid) interneurons. Second, we discovered that many calretinin-positive (CR^+) cells accumulate at the corticostriatal boundary and that fewer CR^+ cells migrate into the neocortex. Third, we showed that the laminar patterns of calbindin-positive (CB^+) interneuron class within the developing neocortex are changed in the *Celsr3* mutant mice. Finally, we demonstrated that expression patterns of neuregulin-1 (*NRG1*) and its receptor *ErbB4* are altered in *Celsr3* mutants. These results suggest that *Celsr3* regulates both the tangential and radial migrations of the GABAergic interneurons in vivo in a class-specific manner in the mouse telencephalon.

MATERIALS AND METHODS

Mutant mice. The detailed protocol for generating the *Celsr3* mutant mice was described in our recent publication (62). Genotyping was performed by PCR with the following primers: CCCCCTGAACCTGAAACATAAAATG, ACTTCA GCACTGCACCCGACTTAC, and GCCCTGCGAGAACTACATGAAATG. Ex-

* Corresponding author. Mailing address: Shanghai Center for Systems Biomedicine, Key Laboratory of Systems Biomedicine (Ministry of Education), Shanghai Jiao Tong University, Shanghai 200240, China. Phone and fax: 86 21 34204300. E-mail: qwu123@gmail.com.

▽ Published ahead of print on 30 March 2009.

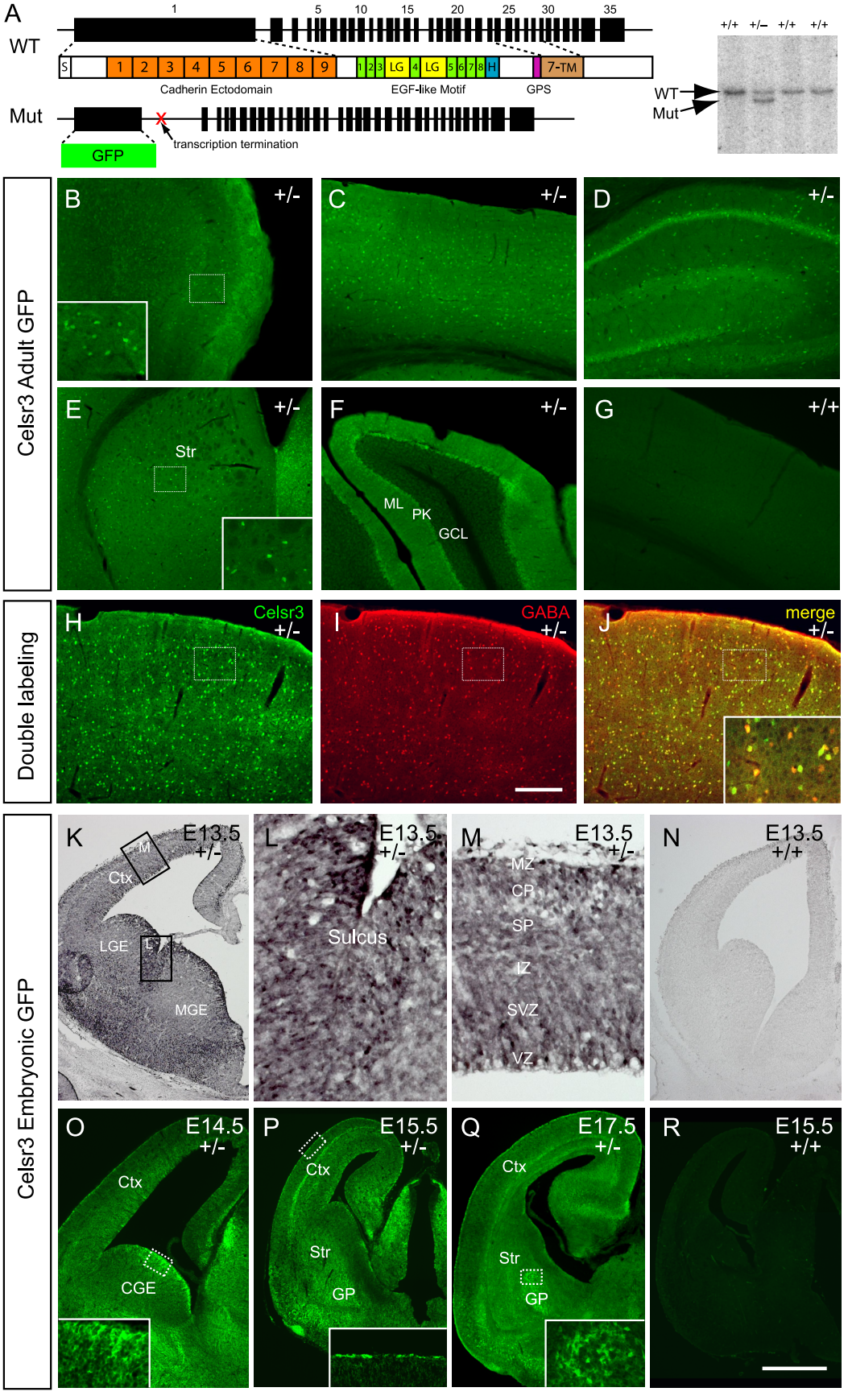
A
WT
Mut
GFP
transcription termination
Cadherin Ectodomain
EGF-like Motif
GPS
7-TM
+/+ +/– +/+ +/+
WT
Mut
Celsr3 Adult GFP
B +/-
C +/-
D +/-
E +/-
Str
F +/-
ML
PK
GCL
G +/+
Double labeling
H Celsr3 +/-
I GABA +/-
J merge +/-
Celsr3 Embryonic GFP
K E13.5 +/-
M
Ctx
LGE
L
MGE
L E13.5 +/-
Sulcus
M E13.5 +/-
MZ
CP
SP
IZ
SVZ
VZ
N E13.5 +/+
O E14.5 +/-
Ctx
CGE
P E15.5 +/-
Ctx
Str
GP
Q E17.5 +/-
Ctx
Str
GP
R E15.5 +/+

periments were approved by the University of Utah Institutional Animal Care and Use Committee and were conducted according to the relevant protocol.

Nissl staining. Postnatal day 0 (P0) brains were sectioned at 30 μm with a sliding microtome (Microm) and mounted to Superfrost Plus slides (Fisher Scientific). After rehydration, the slide was immersed in 1% thionin for 5 min, destained in 50% ethanol, and dried in air. Finally, the sections were dehydrated in a series of 75%, 85%, 95%, and 100% ethanol solutions and cleared in xylene for 10 min; coverslips were applied with mounting medium, and the sections were imaged with a Zeiss microscope.

Immunostaining. Animals at embryonic day 17.5 (E17.5), E18.5, P1, P3, P7, and adult stages were perfused with 4% paraformaldehyde (PFA). The brains were dissected and postfixed in the same fixative for 4 to 6 h. Brains of E13.5 and E15.5 embryos were directly dissected and fixed in 4% PFA overnight. After cryoprotection with 30% sucrose, embryonic brains were embedded in optimal cutting temperature compound (Sakura), sectioned at 12 to 18 μm with a cryostat (Microm), and thaw mounted onto Superfrost Plus slides. The postnatal and adult brains were cut into 35- to 50-μm sections with a microtome and collected in 0.1 M phosphate-buffered saline (PBS). Thaw-mounted or free-floating sections were immunostained. Briefly, after being washed three times in PBS, sections were blocked in 5% normal goat serum–0.3% Triton X-100 for 1 h and incubated with primary antibody prepared with the same blocking solution except without detergent at 4°C overnight. The primary antibodies used were rabbit anti-eGFP (1:1,000; Invitrogen), chicken anti-eGFP (1:1,000; Abcam), mouse anti-neurofilament 165 (1:1,000; 2H3; Developmental Studies Hybridoma Bank), rabbit anti-tyrosine hydroxylase (1:1,000; Covance), rabbit anti-CR (1:2,000; Swant), rabbit anti-CB (1:3,000; Swant), rabbit antiparvalbumin (anti-PV) (1:3,000; Swant), rat antisomatostatin (anti-SST) (1:250; Chemicon), rabbit anti-activated caspase 3 (1:500; Cell Signaling Technology), mouse anti-Tuj1 (1:500; Sigma), mouse anti-MAP2 (1:500; Sigma), mouse anti-islet 1 (1:30; Developmental Studies Hybridoma Bank), and rabbit anti-NRG1 (1:500; Abcam). After sections were washed in PBS, they were incubated with Cy3- or Alexa Fluor 488-conjugated secondary antibody (Jackson ImmunoResearch and Invitrogen) for 1 h at room temperature, washed with PBS, counterstained with 1 μg/ml 4′,6′diamidino-2-phenylindole (DAPI; Invitrogen), washed, and air dried, and coverslips were applied with Fluoromount-G medium (Southern Biotech). GFP immunohistochemistry was done with an ABC Elite kit from the Vector Lab. A terminal uridine deoxynucleotidyltransferase-mediated dUTP nick end labeling assay was performed using a kit (Roche) according to the manual.

Neuronal birth-dating and cell proliferation assay. For neuronal birth dating, dams received bromodeoxyuridine (BrdU) (Sigma) intraperitoneal injections (50 mg/kg five times at 2-h intervals) at E13.5, E15.5, and E16.5. The embryos were then collected at E18.5. The brains were dissected, fixed, cryoprotected, and sectioned as described above. Antigen retrieval was done by boiling sections in 10 mM sodium citrate buffer (pH 6.0) for 10 min. Double labeling of BrdU (1:1,000; G3G4; Developmental Studies Hybridoma Bank) with CR or CB was performed as described above. For cell proliferation analysis, dams received 40 mg/kg BrdU by intraperitoneal injection at E14.5 2 h before the embryos were collected. BrdU-positive cells were counted in standard areas (200 μm by 200 μm) from the caudal ganglionic eminence (CGE) and cortical germinal zone, and the difference between mutants and controls ($n = 5$) was assessed using a two-tailed Student's t test.

Western blotting. Neocortex from the E15.5 *Celsr3* mutants and controls ($n = 6$) was homogenized in RIPA buffer (Sigma) using a Tissue Lyser-II machine (Qiagen). Sixty micrograms of proteins was run on sodium dodecyl sulfate-polyacrylamide gel electrophoresis gels and transferred to a polyvinylidene difluoride membrane. After the membrane was blocked with 10% nonfat dry milk in 0.05 M Tris-buffered saline (pH 7.4), it was incubated overnight with the rabbit anti-NRG1 antibody (1:500; Abcam) at 4°C, washed with Tris-buffered saline, and incubated with horseradish peroxidase-conjugated goat anti-rabbit secondary antibody (1:10,000; Bio-Rad). Signal was detected with an Immun-Star HRP chemiluminescent kit (Bio-Rad). Quantification was done using the NIH ImageJ software (version 1.38).

In situ hybridization. We performed the in situ hybridization as described previously (66). Briefly, brains from E15.5 embryos were fixed in 4% PFA with 2 mM EGTA at 4°C overnight. After being cryoprotected in 30% sucrose, brains were embedded in optimal cutting temperature compound and sectioned at 12 μm. Sections were collected onto the Superfrost slides and pretreated with 4% PFA for 10 min, 1 μg/ml proteinase K for 5 min, acetic anhydride for 10 min, and 1% Triton X-100 for 30 min. Sections were then prehybridized in the hybridization buffer (50% formamide, 5× SSC [1× SSC is 0.15 M NaCl plus 0.015 M sodium citrate], 5× Denhart's, 250 μg/ml *Saccharomyces cerevisiae* tRNA, and 500 μg/ml herring sperm DNA) for 2 h at room temperature, followed by hybridization with RNA probes (1 μg/ml) at 60°C overnight. Sections were washed in 0.2× SSC at 60°C for 1.5 h, blocked in 10% sheep serum, and incubated with the alkaline phosphatase-conjugated sheep antidigoxigenin antibody (1:5,000; Roche) at 4°C overnight. After the washing and equilibration, sections were incubated with the alkaline phosphatase substrate BM purple (Roche). The plasmids for the *Sema3A*, *Sema3F*, *Npn1*, and *Npn2* probes (43) were kindly provided by Tamamaki (Kumamoto University, Japan). The *ErbB4* template (nucleotides 239 to 840 of NM_010154) was amplified by reverse transcription-PCR, cloned into the pCRII-TOPO vector, and sequenced. All probes were synthesized using an in vitro transcription kit from Roche.

In vitro cell migration assay. Germinal zones of the medial ganglionic eminence (MGE) and CGE from the E14.5 *Celsr3* mutant and control littermates were embedded in Matrigel (BD Biosciences) and cultured in minimal essential medium with 10% fetal bovine serum for 48 h. Migration at 2 days in vitro was quantified as described previously (32).

Primary neuronal culture. For in vitro differentiation of interneurons, we followed a published protocol (63). Briefly, brains from P0 *Celsr3*$^{-/-}$ or *Celsr3*$^{+/-}$ littermates were isolated in Hanks' balanced buffer and coronally cut into 500-μm slices. Neocortex was dissected, cut into small pieces, and digested in 0.25% trypsin solution for 15 min at 37°C. Tissues were then gently triturated in plating medium (minimal essential medium, 10% fetal bovine serum, 1 mM glutamine, 10 mM HEPES, pH 7.3). After the cell density was determined with a hematometer, neurons were plated at a density of 2,000/mm^2 onto Permanox eight-well plastic culture plates (Nunc) precoated with polylysine (100 μg/ml) and laminin (5 μg/ml). Half of the medium was replaced with the neurobasal/B27 medium (Invitrogen) containing 10 ng/ml fibroblast growth factor 2 (Promega) the next day and every other following day. At 26 days in vitro cells were fixed in 4% PFA at 4°C for 20 min and subjected to CR, CB, SST, and GABA immunostaining. The CR-, CB-, and SST-positive (SST$^+$) cells were counted at magnifications of ×100 and normalized with the GABA cell numbers. The difference between mutants and controls (five wells; $n = 3$ animals) was assessed using a two-tailed Student's t test.

Imaging and quantification. All images were taken using a Zeiss Axioskop fluorescent microscope equipped with a charge-coupled-device camera. All cell counting was conducted on ×200 (striatal CR$^+$ and cortical CR$^+$ or CB$^+$ cells) or ×400 (olfactory bulb CR$^+$ cells) images with the ImageJ software. Since there is intense CR staining of thalamocortical axons in the subplate (SP) in the controls, we counted only the cells in the subventricular zone (SVZ). In the striatum, we counted only the CR$^+$ cells at the dorsal striatum where fiber staining is much less and where distinct CR$^+$ cells can be easily identified. For cortical CB$^+$ cells counting, we divided the neocortex from marginal zone (MZ) to SP into seven even bins (1). CB$^+$ cells were then counted in each bin. A

FIG. 1. *Celsr3* expression patterns in adult interneurons and embryonic germinal zones. (A) Schematic of the *Celsr3* mutant allele and the DNA blot confirmation. The eGFP reporter was fused in-frame with the first four amino acids and concurrently replaced exons 1 and 2. This introduced a transcription-termination site and a stop codon of eGFP in the *Celsr3* locus, ensuring a null allele. S, signal peptide; GPS, G-protein-coupled receptor proteolytic site; H, hormone receptor domain; LG, laminin-A globular domain; 1-9, 9 cadherin ectodomains; 1-8, eight EGF-like motifs; 7-TM, seven transmembrane segments; WT, wild type; Mut, mutant. (B to G) Fluorescent immunostaining of adult brain sections. *Celsr3* is expressed in a scattered neuronal population characteristic of interneurons in forebrain regions, including the olfactory bulb (B), neocortex (C), hippocampus (D), and striatum (E). (F) Expression of *Celsr3* in the Purkinje cells of the cerebellum. (H to J) Costaining of *Celsr3* and GABA in the neocortex. (K to R) Staining of embryonic brain sections. *Celsr3* is highly expressed in the VZ of LGE, MGE, and CGE at E13.5 and E14.5 (K and O), especially in the LGE-MGE sulcus (L), but the VZ expression is decreased at E15.5 and E17.5 (P and Q). In the developing neocortex, *Celsr3* is mainly expressed in the MZ, SP and SVZ/VZ (K, M, P, and Q). CP, cortical plate; Ctx, cortex; GCL, granule cell layer; GP, globus pallidus; IZ, intermediate zone; ML, molecular layer; PK, Purkinje cell layer; Str, striatum. Bar in panel I, 250 μm for panels B to D and F to J and 500 μm for panel E; bar in panel R, 500 μm for panels K, N, and O, 70 μm for panels L and M, and 850 μm for panels P to R.

two-tailed Student's *t* test was used to estimate the significance of differences between mutants and controls.

RESULTS

Generation of a null allele of *Celsr3* with a knock-in eGFP reporter. The mammalian Pcdh *Celsr* genes have a characteristic genomic organization with 35 exons, of which the first exon is very large and encodes all of the nine ectodomains (Fig. 1A) (60). We inserted an eGFP reporter in the endogenous chromosomal environment under the control of the *Celsr3* transcription and translational signals, replacing the first two exons with a transcription termination site (Fig. 1A) (62). The homozygotes of this *Celsr3* null allele die within several hours after birth, similar to results with a reported allele that deletes exons 19 to 27 and produces mRNA products by splicing the first 18 exons to the frame-shifted exon 28, potentially encoding a secreted protein of 2,262 amino acids with no transmembrane domain (47).

Nissl staining and neurofilament 165 immunostaining confirmed the abnormal gross anatomy of the mutant brain, including the dilation of the lateral ventricle, the shrinkage of the striatum, the thinning of the cerebral wall, and the lack of several major axonal tracts (data not shown) (47). Since a permissive corridor in the ventral telencephalon is required for thalamocortical axonal pathfinding (25), we immunostained the corridor cells with the marker *Islet-1* and found no differences between mutants and controls (data not shown), suggesting no defects in the axonal pathfinding corridor. Finally, we identified two new axonal defects: abnormal axonal fasciculation in the globus pallidus (GP) and aberrant mesencephalic dopaminergic projections to the ventral surface of telencephalon (data not shown).

***Celsr3* expression pattern in the adult and developing brain.** We examined the expression patterns of the *Celsr3* gene by immunofluorescent staining with an anti-eGFP antibody because no green fluorescent signals can be observed directly. Interestingly, *Celsr3* is expressed in scattered populations of cells in various adult forebrain regions including the olfactory bulb, cerebral cortex, hippocampus, and striatum (Fig. 1B to E). In addition, it is also predominantly expressed in the GABAergic Purkinje cells of the cerebellum (Fig. 1F). These results suggest that, in the adult brain, *Celsr3* is prominently expressed in GABAergic-inhibitory neurons. Colabeling with GABA revealed that, in the adult neocortex, Celsr3-GFP and GABA are coexpressed (553 GFP-positive out of 593 GABAergic cells) (Fig. 1H to J). In addition, colabeling with neurochemical markers PV, CR, or SST demonstrated that *Celsr3* is expressed in all three interneuron classes in the adult neocortex (data not shown). However, there is a small fraction of cells in the adult neocortex that are GFP positive but GABA negative (Fig. 1J), suggesting potential additional functions of Celsr3 proteins in non-GABAergic brain cells.

In embryos, *Celsr3* is ubiquitously expressed throughout dorsal and ventral telencephalon (Fig. 1K to R; also data not shown). Consistent with previous in situ data (49), *Celsr3* is, however, predominantly expressed in the progenitor and mantle zones of the ganglionic eminences (GEs, including the lateral GE [LGE], MGE, and CGE) at E13.5 and E14.5 (Fig. 1K and O), especially in the interganglionic sulcus between LGE and MGE (Fig. 1L). These subpallial progenitor zones generate interneuron precursors that tangentially migrate into the developing neocortex (2, 3, 7, 24, 32, 56, 63). In the dorsal telencephalon, *Celsr3* is expressed throughout all layers, but the signal appears to be stronger in the MZ, SP, SVZ, and ventricular zone (VZ) (Fig. 1K, M, and Q). Interestingly, these zones are the major cortical layers in which ventrally born interneurons tangentially migrate within the developing neocortex (3, 4, 24, 45, 57). Together, these results suggest that *Celsr3* plays a role in cortical interneuron development.

To determine whether *Celsr3* is expressed in the migrating immature interneurons, we costained embryonic sections with the interneuron marker of calcium-binding proteins CR or CB. Unfortunately, due to the diffuse signals of *Celsr3* at embryonic stages, we cannot conclude whether *Celsr3* colocalizes with CR or CB. In the postnatal forebrain, the characteristic scattered expression pattern of *Celsr3* emerges around P3 and becomes apparent by P7 (data not shown). Thus, the *Celsr3* expression in the interneurons is gradually upregulated during development.

Decrease of CR^+ cells in the developing neocortex of *Celsr3* mutants. The majority of cortical interneurons can be divided into several largely nonoverlapping classes according to their neurochemical markers such as PV-positive (PV^+), CR^+, and SST^+ cells (19). Recent studies revealed that distinct interneuron classes have different origins in the subpallium. Specifically, the PV^+ interneuron class originates from the MGE (7, 57, 63) while the CR^+ interneuron class originates from the CGE (7, 63). The PV and SST are not expressed in cortical interneurons of the embryonic mice (3, 63); however, CR is expressed in immature interneurons at embryonic stages (12, 23, 27, 53).

To investigate whether there is any defect of interneuron development in the *Celsr3* mutants, we immunostained neocortical sections with a CR antibody. At E18.5 and E17.5 cortices, the CR staining is mostly enriched in the MZ, SP, and SVZ (Fig. 2). CR^+ cells in the MZ are Cajal-Retzius cells (12). There is no obvious difference of CR^+ cells in the MZ between mutants and controls (Fig. 2). CR^+ cells in the SP and SVZ are GABAergic immature interneurons (12), and their numbers are reduced in the mutants compared to controls (Fig. 2A to D, A′ to D′, F to I, and F′ to I′). Because SP contains massive staining of axonal fibers that mask CR^+ cells in control sections, we quantified CR^+ cells in the SVZ only. We found a significant decrease of CR^+ cells at rostral, middle, and caudal levels in the mutant SVZ (Fig. 2E and J). To determine whether this phenotype is caused by increased apoptosis, we performed both the terminal uridine deoxynucleotidyltransferase-mediated dUTP nick end labeling assay and activated caspase 3 immunostaining. We found that there is no increase of apoptotic cells in the mutant neocortical SVZ or in the germinal zones of the subpallium (data not shown). Thus, the decrease in CR^+ cells in the neocortical SVZ likely results from the defects of their migration from subpallium. These results suggested that *Celsr3* plays an important role in the development of the CR^+ interneuron class.

Accumulation of CR^+ cells at the corticostriatal boundary of *Celsr3* mutants. To investigate the reason for the decrease in CR^+ cells in the mutant neocortex, we immunostained the subpallial sections of *Celsr3* mutants and controls. We found a

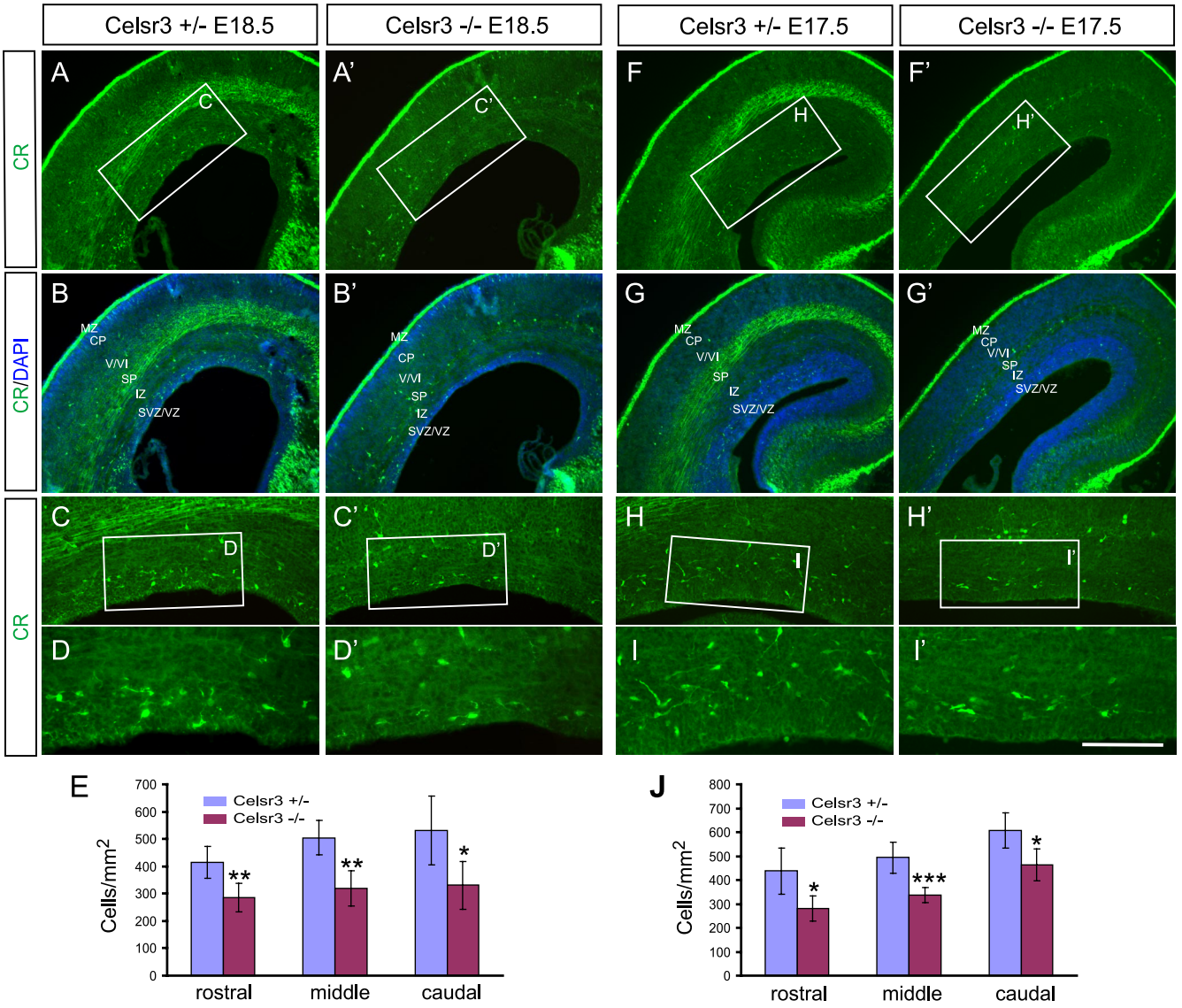

FIG. 2. Decreased CR^+ cells in the developing mutant neocortex. (A to D and A′ to D′) CR staining of the E18.5 neocortex. Counterstaining with DAPI shows distinct cortical layers (B and B′). Note the dilation of the lateral ventricle, the thinning of the neocortex, and the absence of axonal fibers in the mutants. (E) Quantification demonstrated significant decreases of CR^+ cells in the SVZ of the E18.5 mutant forebrain throughout rostral, middle, and caudal levels. (F to I and F′ to I′) Staining of the E17.5 neocortex showed a similar decrease in CR^+ cells to that of E18.5 neocortex. (J) Quantification analyses demonstrated a significant CR^+ cell decrease in the SVZ of the E17.5 mutants. *, $P < 0.05$; **, $P < 0.01$; ***, $P < 0.001$ ($n = 5$; two-tailed Student's t test). CP, cortical plate; IZ, intermediate zone; V/VI, cortical layers V and VI. Bar, 400 μm (A, A′, B, B′, F, F′, G, and G′), 200 μm (C, C′, H, and H′), and 100 μm (D, D′, I, and I′).

striking accumulation of CR^+ cells at the corticostriatal boundary throughout rostral to caudal levels in the E18.5 *Celsr3* mutants (Fig. 3A to D and A′ to D′). These accumulated CR^+ cells have the characteristic morphology of migratory interneurons with an elongated cell body, a long branched or unbranched leading process, and a short trailing process (2, 4, 24, 35, 45). Their leading processes point to multiple directions including dorsomedial, ventrolateral, and dorsolateral. Based on their morphology, these accumulated CR^+ cells appear to be migrating in many directions, among which the dorsomedially oriented CR^+ cells are the most common (44% out of the 154 quantified cells) (Fig. 3D and D′). In addition, staining of sagittal sections (Fig. 4A to D and A′ to D′) revealed accumulated CR^+ cells at the corticostriatal boundary with rostrally or caudally oriented leading processes (Fig. 4E), suggesting that these CR^+ cells are rostrally and caudally migrating interneurons (out of 54 quantified cells, 74% oriented rostrally, and 26% oriented caudally) (Fig. 4). Because the corticostriatal boundary is the crucial turning point for tangential migratory interneurons to populate neocortex, these results strongly suggest that *Celsr3* is required for tangential migration of CR^+ cells from CGE to neocortex in vivo.

At E17.5, there are also large numbers of CR^+ cells accumulated at the corticostriatal boundary (Fig. 3G to J and G′ to J′). These CR^+ cells have the morphology similar to that of E18.5 with leading processes oriented in multiple directions

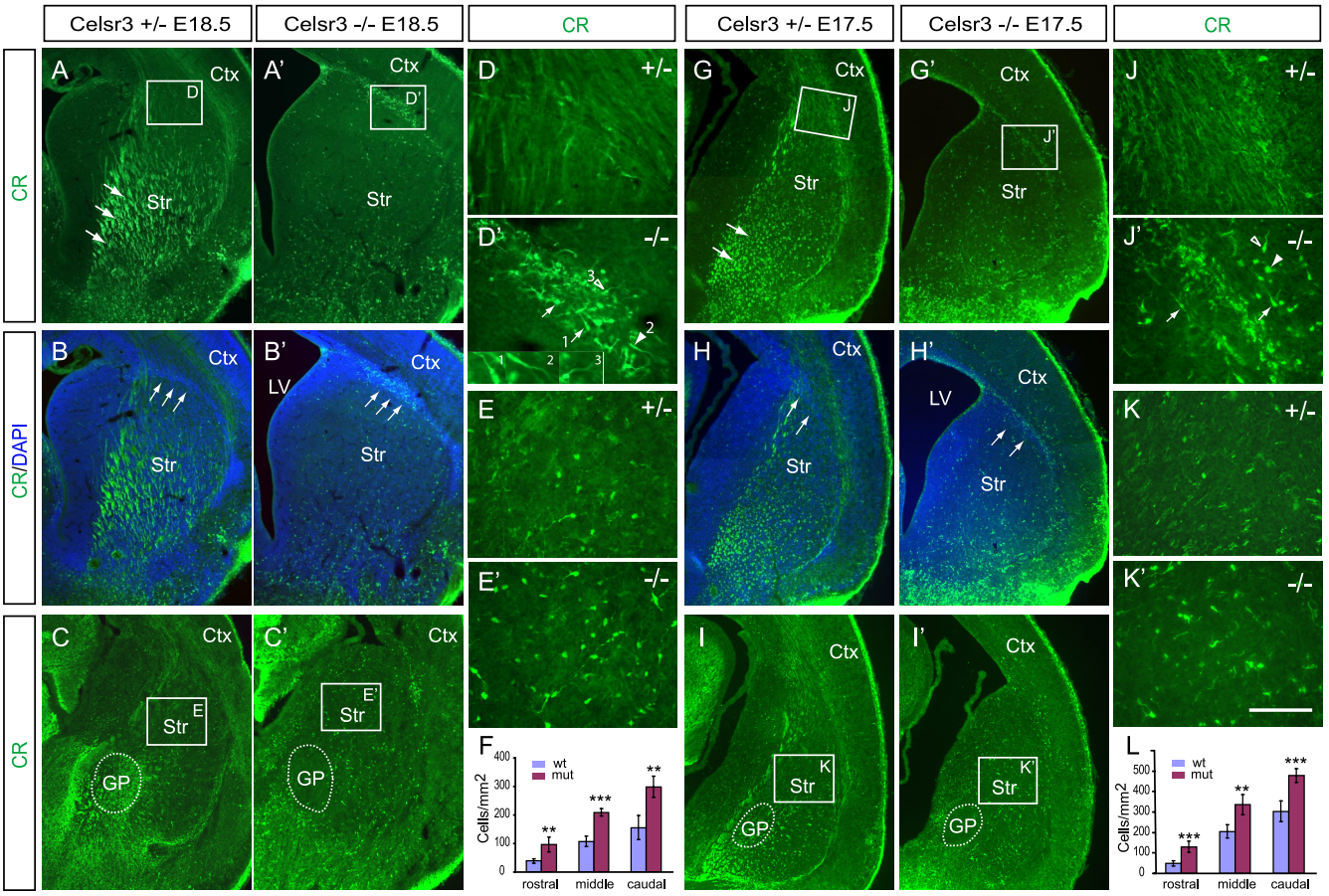

FIG. 3. Accumulation of CR^+ cells at the corticostriatal boundary and in the striatum of *Celsr3* mutants. (A to E and A′ to E′) CR staining of the E18.5 subpallium. Large numbers of CR^+ cells accumulate at the corticostriatal boundary (arrows in panels B and B′) at both rostral (in panels A and A′; counterstained with DAPI in panels B and B′), and caudal (C and C′) levels in *Celsr3* mutants. Note the dilation of the lateral ventricle and the absence of axonal fibers (arrows in panel A) in the mutants (compare panels A′ to C′ with panels A to C). (D and D′) The accumulated CR^+ cells have the morphology characteristic of migratory immature interneurons with leading processes in diverse directions (highlighted in insets), including dorsomedial (arrows), dorsolateral (empty arrowhead), and ventrolateral (arrowhead). (E and E′) Increased CR^+ cells in the E18.5 *Celsr3* mutant striatum. (F) Quantification of striatal CR^+ cells demonstrates significant increases at the rostral, middle, and caudal levels. (G to K and G′ to K′) CR staining of the E17.5 subpallium. The accumulation at the E17.5 corticostriatal boundary is also obvious (compare panels J′ and D′). (L) The striatal CR^+ cells are also increased in the E17.5 mutants throughout rostral, middle, and caudal levels. The data are in means ± standard deviations. A two-tailed Student's *t* test was used for statistics ($n = 5$): **, $P < 0.01$; ***, $P < 0.001$. Ctx, cortex; GP, globus pallidus; LV, lateral ventricle; Str, striatum. Bar, 500 μm (A to C, A′ to C′, G to I, G′ to I′) and 50 μm (D, D′, E, E′, J, J′, K, and K′).

(Fig. 3J and J′). However, the accumulation of CR^+ cells at the corticostriatal boundary is less pronounced than that at E18.5 (Fig. 3D, D′, J, and J′).

Increase of CR^+ interneurons in the developing striatum of *Celsr3* mutants. Striatal interneurons are also generated in the progenitor zone of the subpallium and tangentially migrate into the developing striatum (27). We analyzed the striatal CR^+ interneurons and found an increase in CR^+ cells in the striatum of the E18.5 and E17.5 mutants (Fig. 3A to C, A′ to C′, E, E′, G to I, G′ to I′, K, and K′). The most obvious phenotype of striatal CR staining is the absence of thalamocortical fibers in the mutant. Because of the massive CR staining of the thalamocortical fibers in the ventral part of the striatum in the control mice, we performed a quantitative analysis of only the CR^+ cells in the dorsal part of the striatum where the fiber signals are sparse and CR^+ interneurons are recognizable. The results demonstrated that the CR^+ cell density is significantly increased at rostral, middle, and caudal levels of the *Celsr3* mutant dorsal striatum at both E18.5 and E17.5 (Fig. 3F and L).

To investigate the onset of the tangential migration defects of CR^+ cells, we stained brain sections at earlier developmental stages. At E13.5, there is no obvious difference in CR^+ cell numbers in pallium, subpallium, and the corticostriatal boundary between mutants and controls (Fig. 5A to D and A′ to D′). At E15.5, there is also no significant difference in CR^+ cells in the neocortex; however, there appear to be more CR^+ cells in the mutant striatum and corticostriatal boundary than in the control (Fig. 5E to H and E′ to H′). In addition, based on the direction of the leading processes, we observed that, at the corticostriatal boundary, there are many immature CR^+ cells migrating from the CGE into neocortex in both mutants and controls at E15.5 (data not shown). Finally, in the CGE, 70% of CR^+ cells have the leading process oriented dorsolaterally (151 out of the 215 CR^+ cells quantified) toward the corticostriatal boundary, while in the cortical SVZ, 75% of CR^+ cells

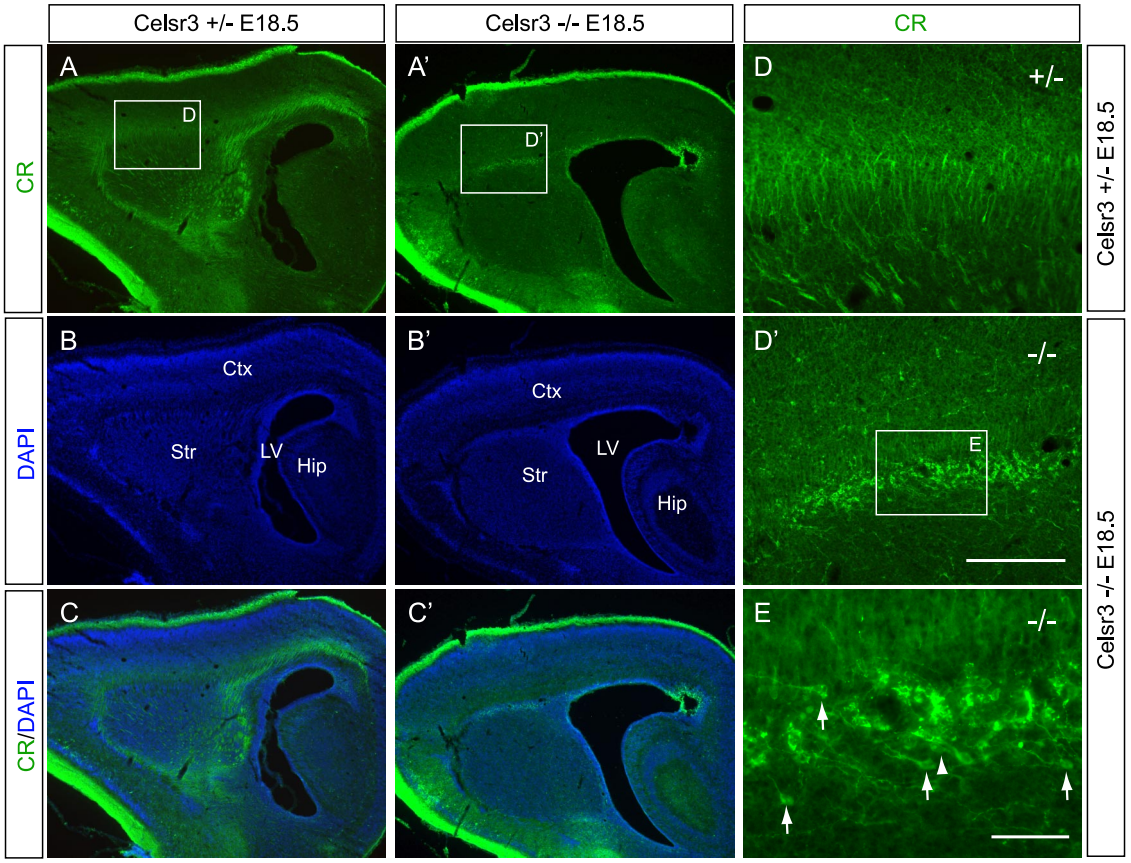

FIG. 4. Sagittal view of the accumulated CR^+ cells in the corticostriatal boundary. (A to E and A′ to D′) CR staining of the sagittal brain sections. The accumulated CR^+ cells are migrating in multiple directions with leading process oriented rostrally (arrows in panel E) or caudally (arrowhead in E). Ctx, cortex; Hip, hippocampus; LV, lateral ventricle; Str, striatum. Bar in panel D′, 800 μm for panels A to C and A′ to C′ and 200 μm for panels D and D′; bar in panel E, 50 μm.

have the leading process oriented dorsomedially (160 out of the 212 CR^+ cells quantified) away from the corticostriatal boundary.

Since the corticostriatal boundary is also important for the rostral migration stream and the lateral cortical stream (8, 41), we performed CR staining of the E18.5 olfactory bulb and basal telencephalic limbic system. Quantification of the CR^+ cells of the olfactory bulb and piriform cortex revealed no significant differences between mutants and controls (data not shown). However, we cannot rule out that some of the accumulated CR^+ cells at the corticostriatal boundary migrate to other brain regions, nor can we rule out that not all accumulated CR^+ cells are from the CGE and destined to the neocortex.

Impaired layering distribution of CB^+ cells within the *Celsr3* mutant neocortex. To address whether other classes of GABAergic interneurons also have migration defects, we stained embryonic brain sections with an antibody against CB, a well-established and widely used GABAergic cortical interneuron marker at embryonic stages (2, 4, 24, 34). At E18.5, CB^+ cells are prominent in the middle tiers of the cortical ribbon of the control mice (Fig. 6A and B) (1, 17). However, CB^+ cells are prominent in the inner tiers of the mutant neocortex in both sagittal and coronal E18.5 sections (Fig. 6A′ and B′), suggesting a layering defect of the cortical CB^+ cells throughout the rostral to caudal and lateral to dorsal levels of the developing neocortex. To facilitate the laminar analysis of the CB^+ cells in the developing neocortex where the layer identification is not clear at this stage, we divided it into seven bins (17). In controls, CB and DAPI colabeling showed that CB^+ cells are concentrated in bins 3 and 4 (Fig. 6C, D, E, I, and J), which roughly corresponds to the inner half of cortical plate and layer V, respectively, while in mutants the signal is more evenly distributed between bins 3 and 7 (Fig. 6C′, D′, E′, I, and J). Quantitative analysis revealed that there are significant differences of the percentage of cells in bin 3 (inner half of the cortical plate) and bins 6 and 7 (inner half of layer VI and SP) at both rostral and caudal levels (Fig. 6I and J). In summary, these results suggest that *Celsr3* plays a role in the radial migration of cortical CB^+ interneurons in vivo.

In contrast to CR^+ cells, there is no accumulation of CB^+ cells at the corticostriatal boundary of the *Celsr3* mutants (Fig. 6B, B′, F, and F′). In addition, the total numbers of CB^+ cells in the neocortex are similar between mutants and controls (data not shown). Therefore, there appear no defects of tangential migration of CB^+ cells from the subpallium to the pallium.

To investigate the time course of the radial migration defects of CB^+ cells in vivo, we studied their distribution at different embryonic stages. At E13.5 and E15.5, the distribution of cor-

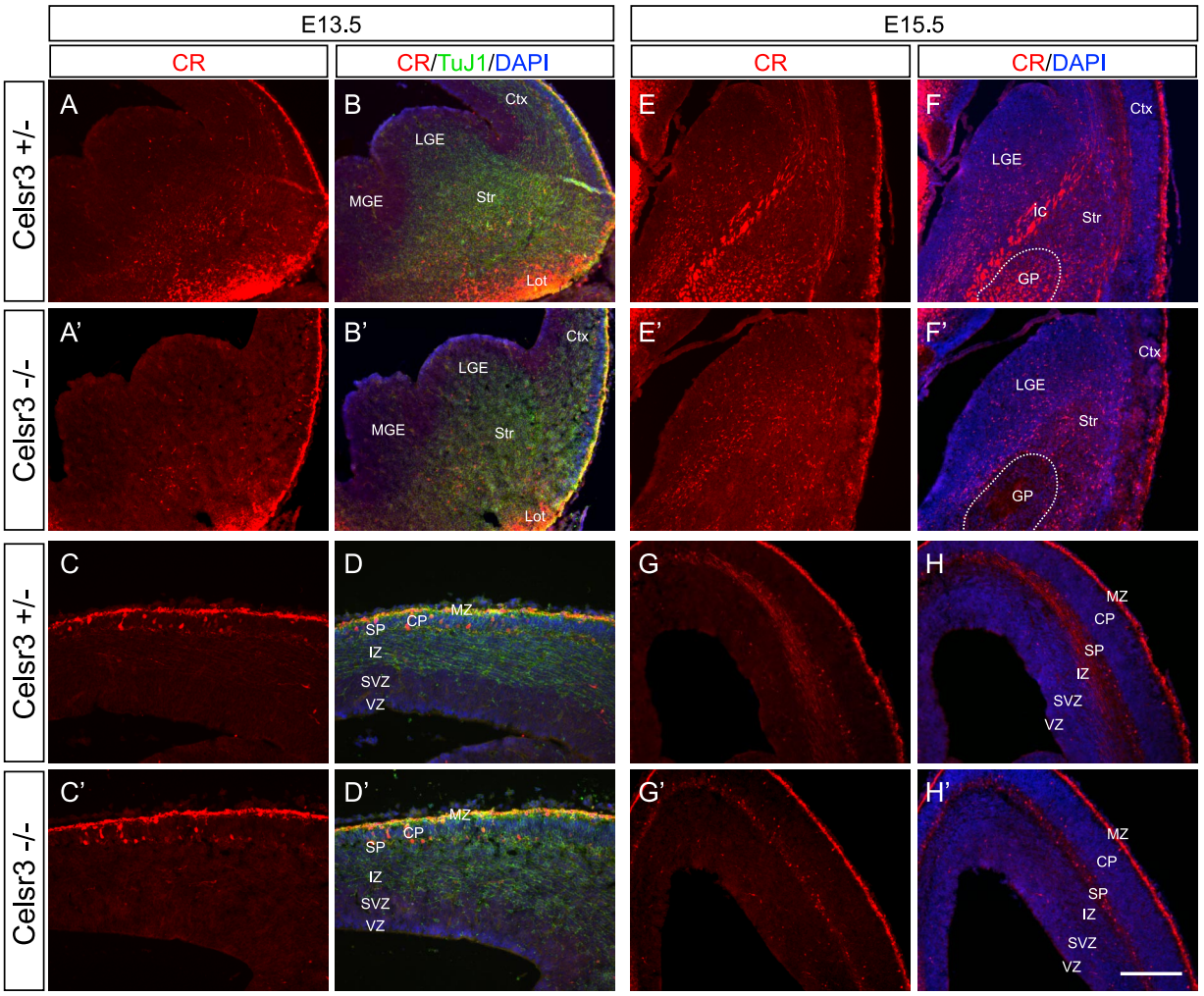

FIG. 5. Development of tangential migration defects of CR^+ cells. No obvious defects of CR^+ cells in E13.5 (A to D and A′ to D′) and E15.5 (E to H and E′ to H′) telencephala of the *Celsr3* mutants were observed. At E13.5, CR expression is low throughout the ventral telencephalic regions except for the lateral olfactory tract (A, A′, B, and B′). The CR staining patterns in the MZ and SP of mutants and controls (C, C′, D, and D′) appeared to be the same. In E15.5 subpallium, there are more CR^+ cells in the mutant striatum and corticostriatal boundary (E′ and F′) than in the control (E and F). Note the missing of CR^+ fibers in the globus pallidus (circled in F and F′) as well as the internal capsule in mutant subpallium (F and F′). In E15.5 pallium, there is no obvious difference between controls and mutants except the absence of CR fiber staining in the SP of the mutants (G, G′, H, and H′). CP, cortical plate; Ctx, cortex; ic, internal capsule; GP, globus pallidus; IZ, intermediate zone; lot, lateral olfactory tract; Str, striatum. Bar, 150 μm (C, C′, D, and D′) and 300 μm (all other panels).

tical CB^+ cells appears normal (Fig. 7A, A′, B, B′, E, E′, F, and F′). At E17.5, we observed more CB^+ cells in the inner tiers of the mutant neocortex than in controls, which is similar to results at E18.5 (Fig. 7I, I′, J, and J′).

In addition to the layering defects of CB^+ cells in the developing neocortex, we also found defects of CB^+ cell distribution in several regions of the E18.5 subpallium (Fig. 6F and F′). First, the clusters of CB^+ cells are known to be abundant in the corticostriatal border at the caudal level (Fig. 6F and G) (17); however, these CB^+ cell clusters are absent in the *Celsr3* mutants (Fig. 6F′ and G′). This phenotype is not obvious at the rostral level where even in the controls very few CB^+ cells could be found (compare Fig. 6B and B′ with F and F′). Second, there is an abnormal cluster of CB^+ cells in the mutant GP (Fig. 6F, F′, H, and H′). To investigate the onset of these two phenotypes, we stained brain sections at E13.5, E15.5, and E17.5 and found that these defects are present at E15.5 and E17.5 but not E13.5 (Fig. 7C, C′, D, D′, G, G′, H, H′, K, K′, L, and L′).

Because the CR^+ and CB^+ cell phenotypes may be caused by the alteration of cell proliferation in the mutants, we performed a cell proliferation assay by BrdU labeling in vivo. Quantification showed that there are no significant changes of BrdU-labeled cell densities in both subpallium and pallium (data not shown).

Late-born CR^+ interneurons accumulate in the corticostriatal boundary. Most cortical CR^+ cells are born between E13.5 and E16.5 (7, 63). To date the birth of the CR^+ cells accumulated in the corticostriatal boundary at E18.5, we injected BrdU at E13.5, E15.5, or E16.5 and performed double staining of BrdU with CR on E18.5 brain sections (Fig. 8). Compared with rare double staining of CR and BrdU in controls, we

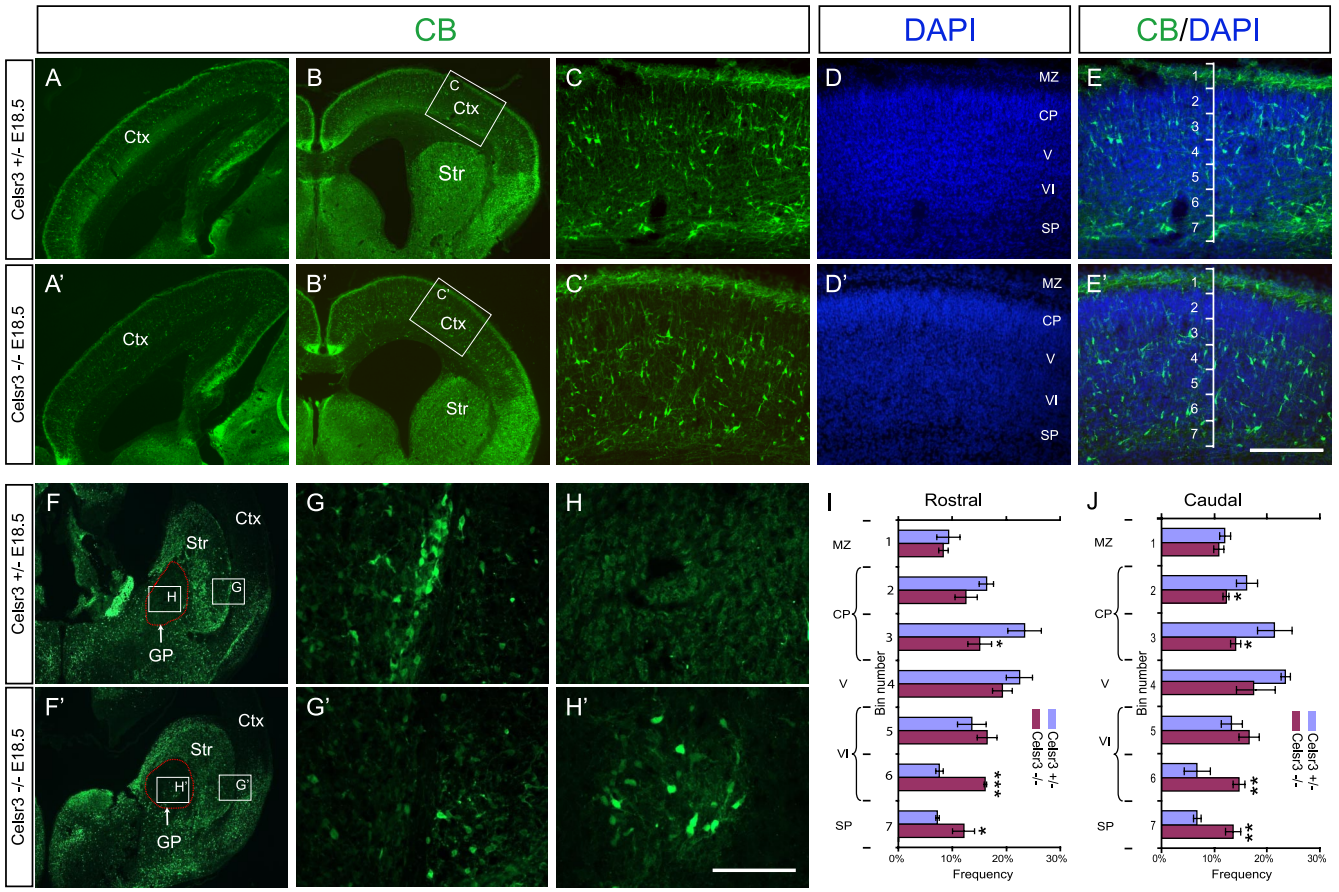

FIG. 6. Impaired radial migration of CB^+ cells in the *Celsr3* mutant neocortex. (A to E and A′ to E′) Cortical CB staining of E18.5 sagittal (A and A′) and coronal (B to E and B′ to E′) sections. For both sagittal and coronal sections, more CB^+ cells are localized at the inner tiers whereas fewer CB^+ cells are localized at the outer tiers in the mutant neocortex. (D and D′) DAPI staining was used to analyze the cortical laminar identity. (E and E′) The cortical region from the MZ to SP was divided into seven even bins, with bin 1 at the MZ and bin 7 at the SP, to facilitate the analyses of the layering distributions of CB^+ cells. (F to H and F′ to H′) CB staining of the E18.5 subpallium. (G and G′) The absence of CB^+ cell clusters at the mutant corticostriatal border. (H and H′) Abnormal distribution of CB^+ cells in the mutant GP. (I and J) Binned quantification of the laminar distribution of CB^+ cells in the rostral and caudal neocortex. Data are presented as means ± standard deviations. *, $P < 0.05$; **, $P < 0.01$; ***, $P < 0.001$ ($n = 3$; two-tailed Student's *t* test). CP, cortical plate; Ctx, cortex; GP, globus pallidus; IZ, intermediate zone; Str, striatum; V/VI, cortical layers V and VI. Bar in panel E′, 200 μm for panels C to E and C′ to E′; bar in panel H′, 800 μm for panels A, A′, B, B′, F, and F′ and 100 μm for panels G, G′, H, and H′.

found that many of the CR^+ cells accumulated at the mutant corticostriatal boundary are colabeled with BrdU injected on E15.5 (Fig. 8F to J and F′ to J′) and E16.5 (Fig. 8K to O and K′ to O′) but few on E13.5 (Fig. 8A to E and A′ to E′). Specifically, quantitative analyses revealed that 11%, 18%, and 4% of the accumulated CR^+ cells are colabeled with BrdU injected on E16.5, E15.5, and E13.5, respectively. These data suggest that the tangential migration of the late-born CR^+ cells is compromised in the *Celsr3* mutants.

Both early- and late-born CB^+ cells have cortical layering defects within the developing neocortex. Double staining of CB and BrdU, injected at E13.5 (Fig. 9A to D and A′ to D′) or E15.5 (Fig. 9F to I and F′ to I′), demonstrated that fewer colabeled cells populate the outer tiers of the mutant neocortex than in controls at E18.5 (Fig. 9). In contrast, more colabeled cells populate the inner tiers of the mutant neocortex (Fig. 9). These differences are statistically significant for both E13.5 (Fig. 9E) and E15.5 (Fig. 9J) of the BrdU injection. These results suggested that CB^+ cells born at both E13.5 and E15.5 are mislocalized in the developing neocortex at E18.5, which is likely due to impaired radical migration of CB^+ cells.

Altered expression pattern of *NRG1* in the developing neocortex and of *ErbB4* in the corticostriatal boundary in *Celsr3* mutants. To gain insight into mechanisms of the *Celsr3* functions in interneuron migration, we examined the expression patterns of several genes that are important in regulating interneuron migration (Fig. 10). We first examined the expression pattern of *NRG1*, a molecule crucial for both tangential and radial migration of interneuron precursors (13, 36). The NRG1 proteins are expressed in two adjacent yet distinct bands sandwiching the SP in the control mice at E15.5 (highlighted in the inset of Fig. 10A), a stage of active radial migration of interneurons in the developing neocortex. However, the *NRG1* expression in the SP is much thinner and appears to be fused together in the mutants (Fig. 10A′). To examine whether the total amount of NRG1 proteins is altered in the mutant neocortex, we performed Western blotting using an anti-

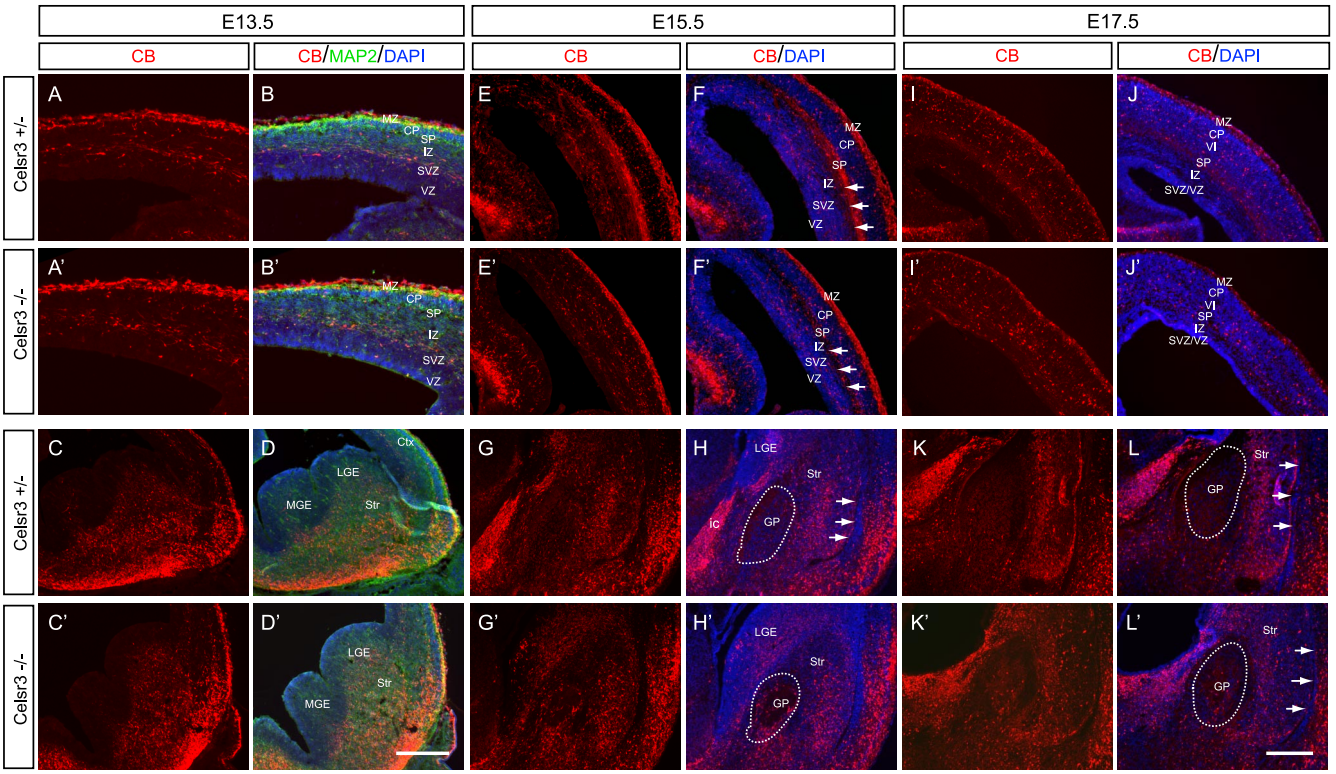

FIG. 7. Development of radial migration defects of CB^+ cells. (A to D and A′ to D′) At E13.5, similar CB labeling was observed in the MZ and the intermediate zone (IZ)/SVZ border of the mutant and control neocortex. Moreover, there is no difference in the CB^+ cells in the subpallium of mutants and controls. Triple staining of CB (red), MAP2 (green), and DAPI (blue) showed that many CB^+ cells also express MAP2. (E to H and E′ to H′) At E15.5, there is no difference in cortical CB^+ cells of controls (E and F) and mutants (E′ and F′). Note that the CB^+ thalamocortical fibers (E; arrows in panel F) are missing in the mutant cortex (arrows in panel F′). In the subpallium, there are many abnormal CB^+ cells in the mutant globus pallidus (G′ and H′) compared with controls (G and H). In addition, many CB^+ cells (G and H [arrows]) normally at the corticostriatal border are missing in the mutants (G′ and H′). (I to L and I′ to L′) At E17.5, in addition to the defects in the globus pallidus and corticostriatal border, the CB^+ cells are abnormally distributed in the inner tiers of the neocortex. CP, cortical plate; Ctx, cortex; ic, internal capsule; GP, globus pallidus; IZ, intermediate zone; Str, striatum; VI, cortical layer VI. Bar in panel D′, 400 μm for panels A, A′, B, and B′ and 200 μm for panels C, C′, D, and D′; in panel L′, 300 μm for panels E to L and E′ to L′.

NRG1 antibody (Fig. 10D) and found that there is no significant difference between the mutants and controls (Fig. 10E). We next examined the expression pattern of ErbB4, the receptor of NRG1, in the E15.5 forebrain. *ErbB4* mRNA is expressed in migratory interneurons at the SVZ of ventral telencephalon in wild-type forebrain (Fig. 10B) (13), and its expression pattern is similar in the mutant SVZ (Fig. 10B′). Interestingly, there are more *ErbB4* signals at the mutant corticostriatal boundary than controls (Fig. 10C and C′), suggesting that the accumulated CR^+ cells may be ErbB4 positive. Unfortunately, the *ErbB4* signal in the neocortex is too weak (Fig. 10B and B′) (13) to determine whether there is any difference of cortical *ErbB4* expression patterns between mutants and controls.

The sorting of striatal and cortical interneurons is regulated by semaphorins (*Sema*) and their receptor neuropilins (*Npn*) (29, 44). To examine whether the semaphorin-neuropilin interaction contributes to the unbalanced distribution of CR^+ between striatum and cortex in the *Celsr3* mutants, we examined the expression patterns of *Sema3A* and *Sema3F* and of *Npn1* and *Npn2* on E15.5 embryos using in situ hybridization. Consistent with previous reports (29, 44), we observed weak expression of *Sema3A* and *Sema3F* in the striatum, prominent expression of *Npn1* in the cortical intermediate zone, and of *Npn2* in the piriform cortex (Fig. 10F to I). However, we found no difference in their expression patterns in the mutants (Fig. 10F′ to I′).

Normal migratory capacity of interneurons from *Celsr3* mutants in vitro. To investigate whether the migratory capacity of interneurons is altered without *Celsr3*, we performed an in vitro migration assay by culturing tissue explants on Matrigel. MGE and CGE explants were cultured in three-dimensional Matrigel matrix for 2 days. The in vitro migratory capacity of MGE and CGE cells was then analyzed (Fig. 11) (32, 56). Migration from *Celsr3* mutant CGE and MGE explants was indistinguishable from controls (Fig. 11A, A′, B, and B′). Consistent with the qualitative observations, quantitative analysis revealed that there is no significant difference in the migrations of CGE and MGE cells from explants at 2 days in vitro between mutants and controls (Fig. 11C), suggesting a normal in vitro migratory capacity for *Celsr3*-deficient MGE and CGE cells.

No differentiation defects of CR^+, PV^+, and SST^+ interneuron classes in vitro. The acquisition of cortical interneuron subtypes is a long, mostly postnatal, developmental process (58). Since the *Celsr3* mutant mice die at birth, we cannot

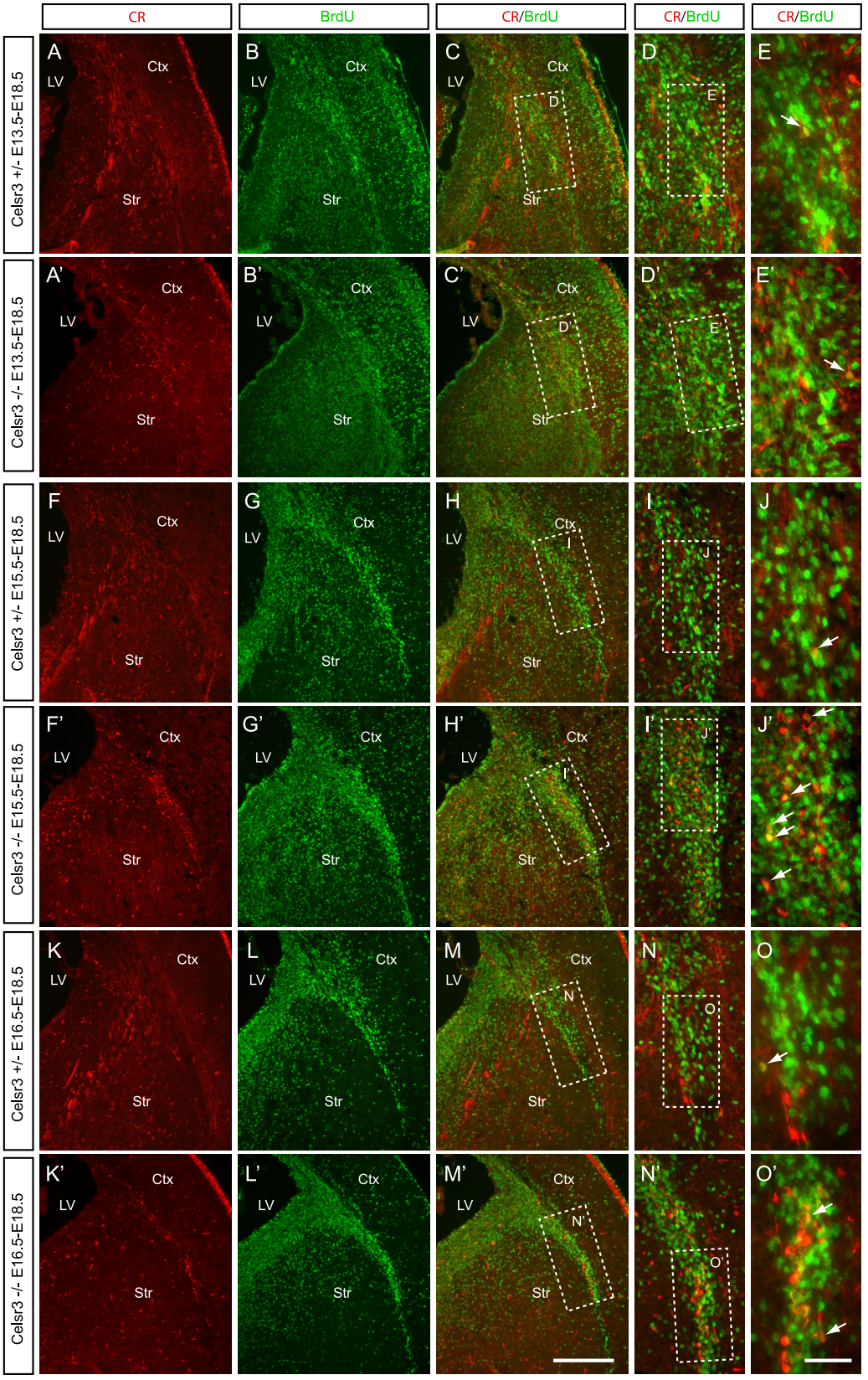

FIG. 8. Birth dating of the accumulated CR^+ cells in the mutant corticostriatal boundary. E18.5 sections were stained for CR (red; A, A′, F, F′, K, and K′) and BrdU (green; B, B′, G, G′, L and L′) which was injected at E13.5 (A to E and A′ to E′), E15.5 (F to J and F′ to J′) or E16.5 (K to O and K′ to O′). Merged view demonstrates that many of CR^+ cells that accumulated in the corticostriatal boundary are colabeled with BrdU injected at E15.5 or E16.5 (H′, I′, M′, and N′ and arrows in panels J′ and O′) but very few at E13.5 (C′ to E′). Ctx, cortex; LV, lateral ventricle; Str, striatum. Bar in panel M′, 150 μm for panels A to C, A′ to C′, F to H, F′ to H′, K to M, and K′ to M′; bar in panel O′, 100 μm for panels D, D′, I, I′, N, and N′ and 50 μm for panels E, E′, J, J′, O and O′.

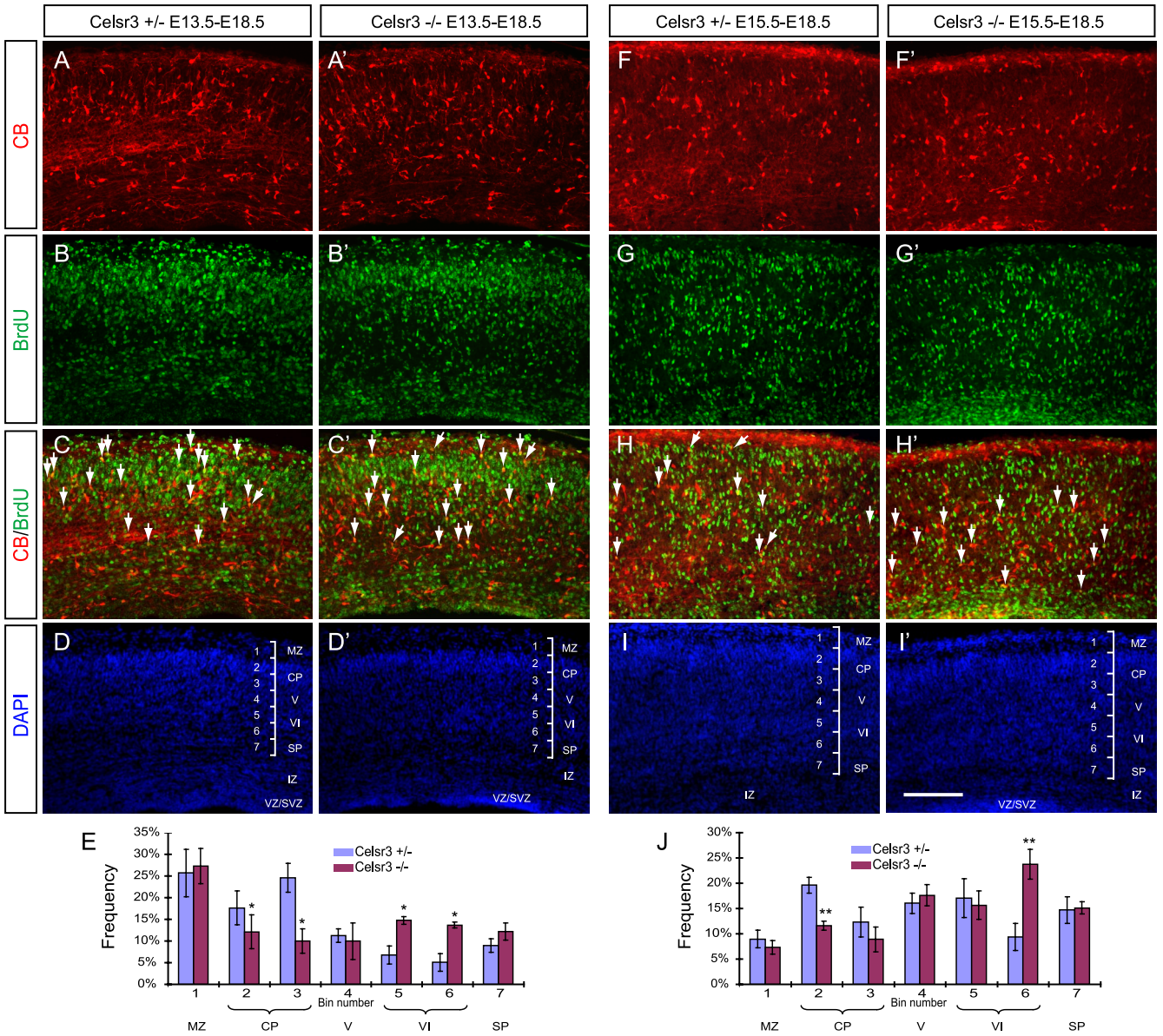

FIG. 9. Birth dating of the mislocalized CB$^+$ cells in the neocortex. E18.5 sections were stained for CB (red; A, A′, F, and F′) and BrdU (green; B, B′, G, and G′) which was injected at E13.5 (A to D and A′ to D′) or E15.5 (F to I and F′ to I′), and the two channels were merged (C, C′, H, and H′). Binned quantification analyses, facilitated by DAPI staining (D, D′, I, and I′), demonstrated significant increases of BrdU-positive CB$^+$ cells in the inner tiers and significant decreases in the outer tiers of the mutant neocortex at both E13.5 (E) and E15.5 (J). CP, cortical plate; IZ, intermediate zone; V/VI, cortical layers V and VI. *, $P < 0.05$; **, $P < 0.01$ ($n = 5$; two-tailed Student's t test). Bar, 150 μm.

investigate the role of *Celsr3* in the differentiation of CR$^+$, PV$^+$, and SST$^+$ cells in vivo. Therefore, we studied their differentiation in vitro by culturing P0 neocortical neurons for 4 weeks when their neurochemical characteristics resemble those of mature interneurons. We stained cultured neurons with the anti-CR, -PV, -SST, and -GABA antibodies. We found that all three classes of interneurons are present in primary cultures without *Celsr3*. Moreover, the ratio of CR$^+$, PV$^+$, and SST$^+$ cells to GABA-positive cells is similar between mutants and controls, suggesting that interneuron differentiation proceeds normally in vitro without Celsr3 proteins (data not shown).

DISCUSSION

Members of the cadherin family play important roles in neurodevelopment in the vertebrate central nervous system (21, 42, 64). In the spinal cord, type II cadherins regulate specific segregation of motor neuron pools (37). Moreover, clustered *Pcdh*γ genes are essential for the survival of spinal interneurons (55). In the hindbrain, disruption of classic cadherins causes the slowdown of the tangential migration of the murine precerebellar neurons both in vitro and in vivo (46). Here, we provide genetic evidence that the murine *Celsr3* gene, a member of the nonclustered *Pcdh* subfamily, is required for

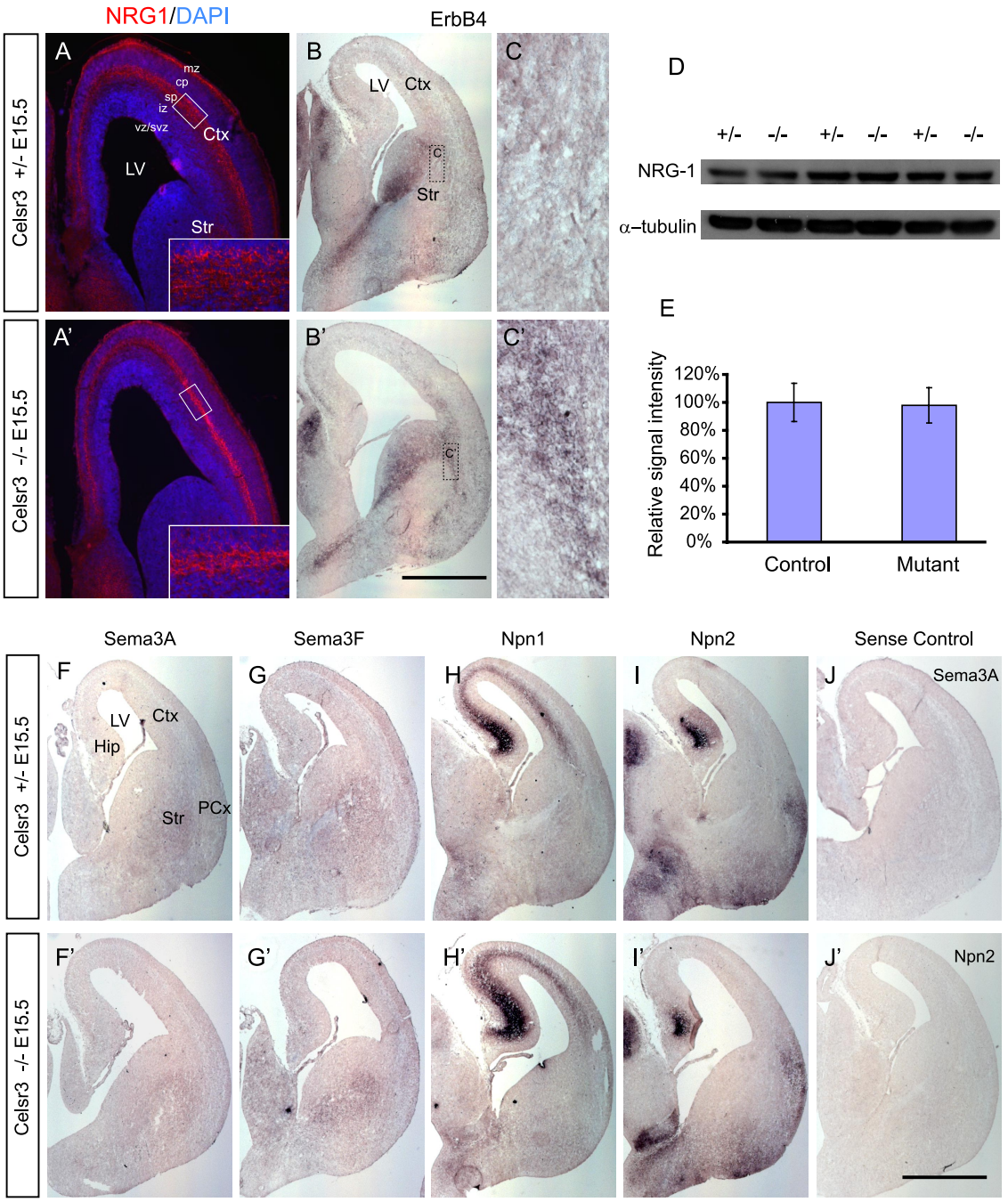

FIG. 10. Dysregulation of *NRG1* and *ErbB4* expression patterns in the developing forebrain of *Celsr3* mutants. NRG1 immunostaining of the E15.5 control (A) and mutant (A′) neocortex, counterstained with DAPI. NRG1-expressing strip is much thinner in mutants (A′) than in controls (A; highlighted in inset). The expression of *ErbB4* is increased in the mutant corticostriatal boundary (B, B′, C, and C′). The total amounts of NRG1 protein are similar in mutants and controls (D and E) ($P = 0.81$ [$n = 6$] with a two-tailed Student's t test). The expression patterns of *Sema3A*, *Sema3F*, *Npn1*, and *Npn2* are the same in mutants and controls (F to J and F′ to J′). CP, cortical plate; Ctx, cortex; Hip, hippocampus; IZ, intermediate zone; LV, lateral ventricle; PCx, piriform cortex; Str, striatum. Bar in panel B′, 650 μm for panels A and A′, 1,000 μm for panels B and B′, and 125 μm for panels C and C′; bar in panel J′, 1,000 μm for panels F to J and F′ to J′.

interneuron migration in the developing forebrain. There are three *Celsr* protocadherin genes in the mammalian genomes (20, 48, 60). Given their identical genomic organizations (48, 60) and their high sequence similarity to the *Drosophila* Fmi protein (51), the three mammalian *Celsr* genes are clearly duplicated from an ancestral *Fmi*-like gene.

The duplication-degeneration-complementation model of gene evolution posits that duplicated genes are expressed in subdomains of the ancestral expression domain and accomplish discrete subfunctions of the ancestral gene (14). The *Drosophila Fmi* is broadly expressed in the epithelium and nervous system and plays multiple roles in tissue morphogen-

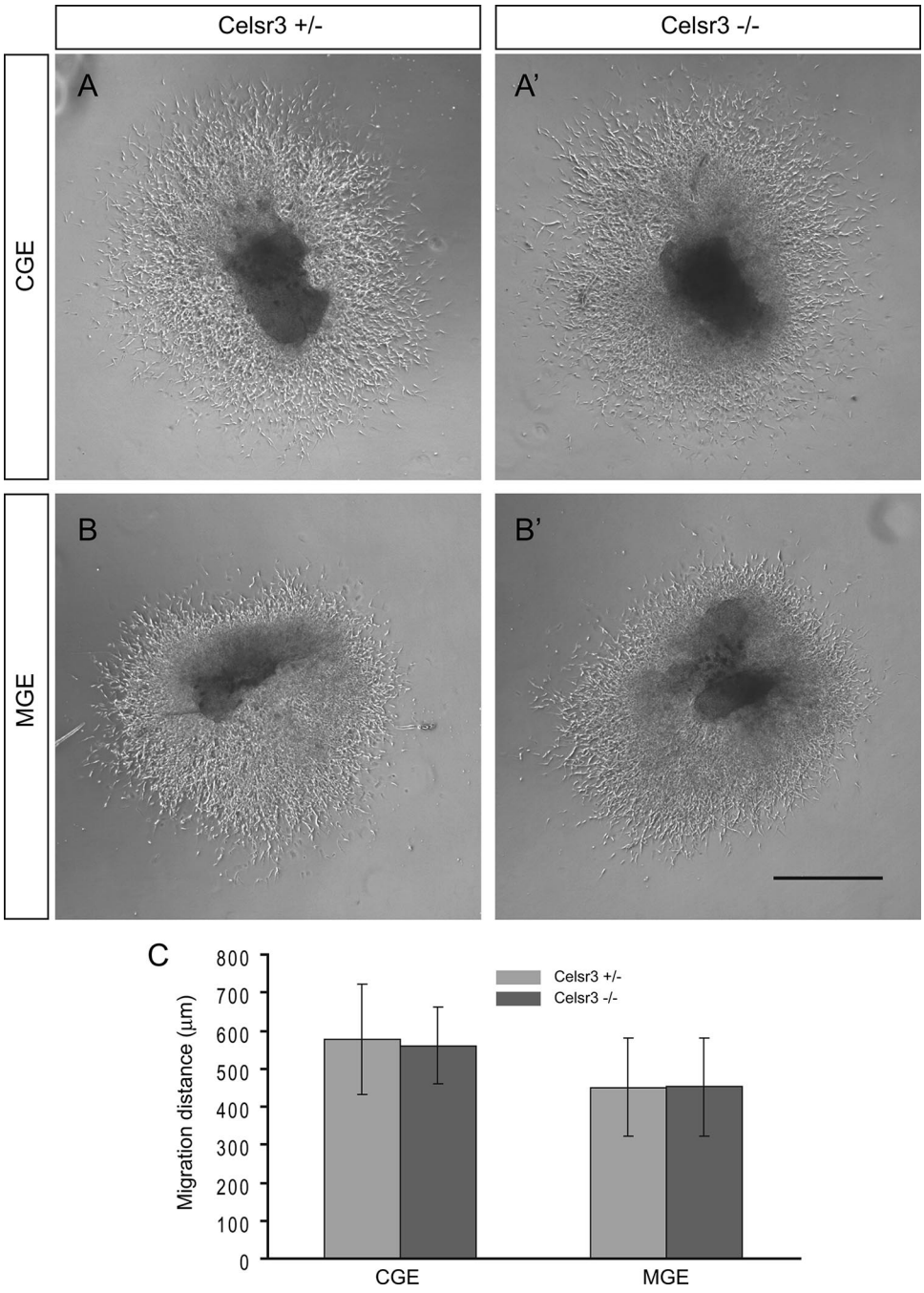

FIG. 11. Normal migratory capacity of CGE and MGE cells from *Celsr3* mutants in Matrigel. CGE and MGE explants from mutants (A′ and B′) and controls (A and B) were cultured in vitro for 2 days in Matrigel, and the distances of cell migration away from the edge of mutant and control explants were quantified (C). Significance was determined with a two-tailed Student's *t* test: $P = 0.78$ for CGE, and $P = 0.98$ for MGE ($n = 8$ for mutants and $n = 12$ for controls). Bar, 500 μm.

esis. Consistent with the duplication-degeneration-complementation model of gene duplication, the three vertebrate paralogs *Celsr1-3* are expressed in largely complementary patterns in the developing nervous system (15, 38, 48) and appear to accomplish the three *Fmi* subfunctions of PCP, dendritic maturation, and axonal tract development, respectively (11, 40, 47). However, our genetic analyses revealed a novel function of *Celsr3* in tangential migration of CR^+ cells from subpallium as well as radial migration of CB^+ interneuron class within the developing neocortex. In addition, a recent in vitro study demonstrated that *Celsr3* suppresses the growth of neurites (39). Therefore, the mammalian *Celsr3* has evolved multiple functions. Finally, mutations of the *Pcdh Celsr2* impair facial motor neuron migration in the zebrafish hindbrain (54). Thus, the vertebrate *Pcdh Celsr* genes have acquired novel functions in neuronal migration.

Cell migration is a fundamental process in vertebrate embryonic development, tissue morphogenesis, and cerebral cortical lamination (5, 28). In the developing mammalian forebrain, most cortical interneurons are born in the subpallium and migrate tangentially to populate various cortical regions in the pallium (10, 28, 58). Disruption of the development and function of diverse interneuron classes contributes to major neuropsychiatric diseases, including autism, schizophrenia, depression, and anxiety disorders (58). The subpallial MGE produces PV^+ fast-spiking multipolar interneurons (7, 57, 63) while the CGE generates primarily CR^+ regular-spiking bipolar or bitufted interneurons (7, 63). The identity of cortical interneuron subtypes is determined at their birth locations and is not influenced by the microenvironments encountered during migration or at their final laminar positions (7, 32, 59, 63). Using a novel deletion allele of the *Pcdh Celsr3* gene with an eGFP knock-in reporter, we found that *Celsr3* is highly expressed in the VZ but is expressed at a lower level in the SVZ of the subpallium (Fig. 1), consistent with previous in situ data (49). Given the cell adhesion properties of the Fmi/Celsr proteins (51), *Celsr3* may serve as a cell surface marker for certain types of neural progenitor cells, probably interneuron progenitors. The VZ expression of *Celsr3* is very similar to that of the transcription factor *Mash1* and *Gsh2* (9, 50), both of which play an important role in interneuron development. In the developing neocortex, *Celsr3* is expressed prominently in MZ, SP, and SVZ (Fig. 1), which are major zones for tangential migration of cortical interneurons (3, 4, 10, 24, 28, 45, 57), consistent with a role of *Celsr3* in interneuron migration. Finally, *Celsr3* is prominently expressed in the GABAergic-inhibitory interneurons in the postnatal and adult brain. In summary, the expression pattern of *Celsr3* suggests that it plays a role in interneuron development.

Migratory interneurons have to pass through the critical corticostriatal boundary to enter the developing dorsal neocortex (28, 31). The underlying mechanism for tangential migration of interneurons from the subpallium, across the crucial corticostriatal boundary, and into the developing neocortex is poorly understood (10, 28, 58). Here, we report novel defects of tangential migration of CR^+ cells from the subpallium to the developing neocortex in the *Celsr3* homozygous mutants. In contrast to CR^+ cells from CGE, we find no tangential migration defects of CB^+ cells from MGE, suggesting that the tangential migration mechanisms for distinct classes of interneurons are different. Many transcription factors have been found to play important roles in the tangential migration of interneurons (28, 58). However, to our knowledge, *Celsr3* is the first cell adhesion molecule found to be required for interneuron migration in the developing forebrain. We have studied the expression patterns of Mash1 and Pax6 proteins in the *Celsr3* mutant forebrain and found no differences in comparison to controls (data not shown). Nevertheless, it will be very interesting to determine whether the cell adhesion gene *Celsr3* is regulated by these transcription factors.

Several scenarios could explain the observed CR^+ cell migration defects in the *Celsr3* mutants. First, given the important role of secretin receptor-type G-protein-coupled receptors in neuronal differentiation, the property of CR^+ cells generated from the *Celsr3*-inactivated CGE could be altered, resulting in the loss of their ability to follow proper guidance cues during migration. In this scenario, *Celsr3* has a cell-autonomous function. Second, the migratory microenvironments at the corticostriatal boundary could be altered in the mutant and thus be unable to guide CR^+ cells for proper tangential migration. In this scenario, *Celsr3* has a non-cell-autonomous function. Finally, as cell surface molecules, the Celsr3 proteins could have both cell-autonomous and non-cell-autonomous functions. Given the known homophilic cell adhesion activity of the homologous Fmi proteins (51), it is tempting to speculate that the disruption of the adhesive interaction between CR^+ cells and thalamocortical axonal fibers may be the reason for the accumulation of CR^+ cells at the mutant corticostriatal boundary. The question of whether *Celsr3* functions in the CR^+ cell migration cell-autonomously, non-cell-autonomously, or both, might be resolved by future transplantation experiments.

Interneurons switch from tangential migration to radial migration to incorporate into their final laminar positions after arrival at appropriate neocortical regions (26, 45, 52); however, little is known about the molecular mechanisms of interneuron radial migration (4, 17, 22, 33). The defects of the laminar layering of CB^+ interneurons in the mutant neocortex suggest a role of *Celsr3* in the radial migration of CB^+ cells in vivo. These layering defects of CB^+ cells in the *Celsr3* mutants are strikingly similar to the radial migration defects of CB^+ cortical interneurons in mice with deletion of the doublecortin or doublecortin-like kinase genes (17). It will be interesting to determine whether these microtubule-associated proteins function in the *Celsr3* cytoplasmic signaling pathway. The NRG1 and its receptor ErbB4 play an important role in interneuron tangential and radial migration (13, 36), and their mutations in humans associate with schizophrenia (30). Consistent with cortical layering defects of CB^+ cells, the NRG1 expression pattern in the neocortex appears to be disrupted in the *Celsr3* mutants (Fig. 10). Because the NRG1 antibody, which is produced with a synthetic peptide from the EGF-like domain, recognizes only a subset of NRG1 protein isoforms, the actual alteration of NRG1 expression patterns in *Celsr3* mutants may be more prominent. In addition, in situ hybridization experiments revealed that the ErbB4-positive cells accumulate in the corticostriatal boundary of *Celsr3* mutants compared to controls (Fig. 10), suggesting altered migration of ErbB4-positive interneurons in the absence of *Celsr3*. Because both radial and tangential migration of interneurons is compromised when the NRG1/ErbB4 signaling is disrupted (13, 36), our data are consistent with the idea that cell adhesion protein Celsr3 regulates interneuron migration through *NRG1* and *ErbB4* signaling.

ACKNOWLEDGMENTS

We thank N. Tamamaki for the *Sema3A*, *Sema3F*, *Npn1*, and *Npn2* plasmids; S. Y. Ahn for technical assistance; G. Fishell and J. L. Rubenstein for suggestions; and R. A. McKnight, L. C. Murtaugh, and J. L. Rubenstein for critical comments.

This work was supported by grant RSG-03-034-01-DDC from the American Cancer Society and 2009CB918700 from the MOST of China (to Q.W.). Q.W. is a March of Dimes Basil O'Connor Scholar.

REFERENCES

1. **Alcántara, S., E. Pozas, C. F. Ibañez, and E. Soriano.** 2006. BDNF-modulated spatial organization of Cajal-Retzius and GABAergic neurons in the marginal zone plays a role in the development of cortical organization. Cereb. Cortex **16:**487–499.

2. **Anderson, S. A., D. D. Eisenstat, L. Shi, and J. L. Rubenstein.** 1997. Interneuron migration from basal forebrain to neocortex: dependence on *Dlx* genes. Science **278:**474–476.
3. **Anderson, S. A., O. Marín, C. Horn, K. Jennings, and J. L. Rubenstein.** 2001. Distinct cortical migrations from the medial and lateral ganglionic eminences. Development **128:**353–363.
4. **Ang, E. S., Jr., T. F. Haydar, V. Gluncic, and P. Rakic.** 2003. Four-dimensional migratory coordinates of GABAergic interneurons in the developing mouse cortex. J. Neurosci. **23:**5805–5815.
5. **Ayala, R., T. Shu, and L. H. Tsai.** 2007. Trekking across the brain: the journey of neuronal migration. Cell **128:**29–43.
6. **Benson, D. L., D. R. Colman, and G. W. Huntley.** 2001. Molecules, maps and synapse specificity. Nat. Rev. Neurosci. **2:**899–909.
7. **Butt, S. J., M. Fuccillo, S. Nery, S. Noctor, A. Kriegstein, J. G. Corbin, and G. Fishell.** 2005. The temporal and spatial origins of cortical interneurons predict their physiological subtype. Neuron **48:**591–604.
8. **Carney, R. S., T. B. Alfonso, D. Cohen, H. Dai, S. Nery, B. Stoica, J. Slotkin, B. S. Bregman, G. Fishell, and J. G. Corbin.** 2006. Cell migration along the lateral cortical stream to the developing basal telencephalic limbic system. J. Neurosci. **26:**11562–11574.
9. **Corbin, J. G., N. Gaiano, R. P. Machold, A. Langston, and G. Fishell.** 2000. The *Gsh2* homeodomain gene controls multiple aspects of telencephalic development. Development **127:**5007–5020.
10. **Corbin, J. G., S. Nery, and G. Fishell.** 2001. Telencephalic cells take a tangent: non-radial migration in the mammalian forebrain. Nat. Neurosci. **4**(Suppl.)**:**1177–1182.
11. **Curtin, J. A., E. Quint, V. Tsipouri, R. M. Arkell, B. Cattanach, A. J. Copp, D. J. Henderson, N. Spurr, P. Stanier, E. M. Fisher, P. M. Nolan, K. P. Steel, S. D. Brown, I. C. Gray, and J. N. Murdoch.** 2003. Mutation of *Celsr1* disrupts planar polarity of inner ear hair cells and causes severe neural tube defects in the mouse. Curr. Biol. **13:**1129–1133.
12. **Del Río, J. A., A. Martínez, C. Auladell, and E. Soriano.** 2000. Developmental history of the subplate and developing white matter in the murine neocortex. Neuronal organization and relationship with the main afferent systems at embryonic and perinatal stages. Cereb. Cortex **10:**784–801.
13. **Flames, N., J. E. Long, A. N. Garratt, T. M. Fischer, M. Gassmann, C. Birchmeier, C. Lai, J. L. Rubenstein, and O. Marín.** 2004. Short- and long-range attraction of cortical GABAergic interneurons by neuregulin-1. Neuron **44:**251–261.
14. **Force, A., M. Lynch, F. B. Pickett, A. Amores, Y. L. Yan, and J. Postlethwait.** 1999. Preservation of duplicate genes by complementary, degenerative mutations. Genetics **151:**1531–1545.
15. **Formstone, C. J., and P. F. Little.** 2001. The *flamingo*-related mouse *Celsr* family (*Celsr1-3*) genes exhibit distinct patterns of expression during embryonic development. Mech. Dev. **109:**91–94.
16. **Formstone, C. J., and I. Mason.** 2005. Combinatorial activity of Flamingo proteins directs convergence and extension within the early zebrafish embryo via the planar cell polarity pathway. Dev. Biol. **282:**320–335.
17. **Friocourt, G., J. S. Liu, M. Antypa, S. Rakić, C. A. Walsh, and J. G. Parnavelas.** 2007. Both doublecortin and doublecortin-like kinase play a role in cortical interneuron migration. J. Neurosci. **27:**3875–3883.
18. **Gao, F. B., M. Kohwi, J. E. Brenman, L. Y. Jan, and Y. N. Jan.** 2000. Control of dendritic field formation in *Drosophila*: the roles of *flamingo* and competition between homologous neurons. Neuron **28:**91–101.
19. **Gonchar, Y., and A. Burkhalter.** 1997. Three distinct families of GABAergic neurons in rat visual cortex. Cereb. Cortex **7:**347–358.
20. **Hadjantonakis, A. K., W. J. Sheward, A. J. Harmar, L. de Galan, J. M. Hoovers, and P. F. Little.** 1997. *Celsr1*, a neural-specific gene encoding an unusual seven-pass transmembrane receptor, maps to mouse chromosome 15 and human chromosome 22qter. Genomics **45:**97–104.
21. **Halbleib, J. M., and W. J. Nelson.** 2006. Cadherins in development: cell adhesion, sorting, and tissue morphogenesis. Genes Dev. **20:**3199–3214.
22. **Hammond, V., E. So, J. Gunnersen, H. Valcanis, M. Kalloniatis, and S. S. Tan.** 2006. Layer positioning of late-born cortical interneurons is dependent on *Reelin* but not *p35* signaling. J. Neurosci. **26:**1646–1655.
23. **Kohwi, M., M. A. Petryniak, J. E. Long, M. Ekker, K. Obata, Y. Yanagawa, J. L. Rubenstein, and A. Alvarez-Buylla.** 2007. A subpopulation of olfactory bulb GABAergic interneurons is derived from *Emx1*- and *Dlx5/6*-expressing progenitors. J. Neurosci. **27:**6878–6891.
24. **Lavdas, A. A., M. Grigoriou, V. Pachnis, and J. G. Parnavelas.** 1999. The medial ganglionic eminence gives rise to a population of early neurons in the developing cerebral cortex. J. Neurosci. **19:**7881–7888.
25. **López-Bendito, G., A. Cautinat, J. A. Sánchez, F. Bielle, N. Flames, A. N. Garratt, D. A. Talmage, L. W. Role, P. Charnay, O. Marín, and S. Garel.** 2006. Tangential neuronal migration controls axon guidance: a role for neuregulin-1 in thalamocortical axon navigation. Cell **125:**127–142.
26. **López-Bendito, G., K. Sturgess, F. Erdélyi, G. Szabó, Z. Molnár, and O. Paulsen.** 2004. Preferential origin and layer destination of GAD65-GFP cortical interneurons. Cereb. Cortex **14:**1122–1133.
27. **Marín, O., S. A. Anderson, and J. L. Rubenstein.** 2000. Origin and molecular specification of striatal interneurons. J. Neurosci. **20:**6063–6076.
28. **Marín, O., and J. L. Rubenstein.** 2003. Cell migration in the forebrain. Annu. Rev. Neurosci. **26:**441–483.
29. **Marín, O., A. Yaron, A. Bagri, M. Tessier-Lavigne, and J. L. Rubenstein.** 2001. Sorting of striatal and cortical interneurons regulated by semaphorin-neuropilin interactions. Science **293:**872–875.
30. **Mei, L., and W. C. Xiong.** 2008. Neuregulin 1 in neural development, synaptic plasticity and schizophrenia. Nat. Rev. Neurosci. **9:**437–452.
31. **Molnár, Z., and A. B. Butler.** 2002. The corticostriatal junction: a crucial region for forebrain development and evolution. Bioessays **24:**530–541.
32. **Nery, S., G. Fishell, and J. G. Corbin.** 2002. The caudal ganglionic eminence is a source of distinct cortical and subcortical cell populations. Nat. Neurosci. **5:**1279–1287.
33. **Pla, R., V. Borrell, N. Flames, and O. Marín.** 2006. Layer acquisition by cortical GABAergic interneurons is independent of *Reelin* signaling. J. Neurosci. **26:**6924–6934.
34. **Pleasure, S. J., S. Anderson, R. Hevner, A. Bagri, O. Marín, D. H. Lowenstein, and J. L. Rubenstein.** 2000. Cell migration from the ganglionic eminences is required for the development of hippocampal GABAergic interneurons. Neuron **28:**727–740.
35. **Polleux, F., K. L. Whitford, P. A. Dijkhuizen, T. Vitalis, and A. Ghosh.** 2002. Control of cortical interneuron migration by neurotrophins and PI3-kinase signaling. Development **129:**3147–3160.
36. **Poluch, S., and S. L. Juliano.** 2007. A normal radial glial scaffold is necessary for migration of interneurons during neocortical development. Glia **55:**822–830.
37. **Price, S. R., N. V. De Marco Garcia, B. Ranscht, and T. M. Jessell.** 2002. Regulation of motor neuron pool sorting by differential expression of type II cadherins. Cell **109:**205–216.
38. **Shima, Y., N. G. Copeland, D. J. Gilbert, N. A. Jenkins, O. Chisaka, M. Takeichi, and T. Uemura.** 2002. Differential expression of the seven-pass transmembrane cadherin genes *Celsr1-3* and distribution of the Celsr2 protein during mouse development. Dev. Dyn. **223:**321–332.
39. **Shima, Y., S. Y. Kawaguchi, K. Kosaka, M. Nakayama, M. Hoshino, Y. Nabeshima, T. Hirano, and T. Uemura.** 2007. Opposing roles in neurite growth control by two seven-pass transmembrane cadherins. Nat. Neurosci. **10:**963–969.
40. **Shima, Y., M. Kengaku, T. Hirano, M. Takeichi, and T. Uemura.** 2004. Regulation of dendritic maintenance and growth by a mammalian 7-pass transmembrane cadherin. Dev. Cell **7:**205–216.
41. **Stenman, J., H. Toresson, and K. Campbell.** 2003. Identification of two distinct progenitor populations in the lateral ganglionic eminence: implications for striatal and olfactory bulb neurogenesis. J. Neurosci. **23:**167–174.
42. **Takeichi, M.** 2007. The cadherin superfamily in neuronal connections and interactions. Nat. Rev. Neurosci. **8:**11–20.
43. **Tamamaki, N., K. Fujimori, Y. Nojyo, T. Kaneko, and R. Takauji.** 2003. Evidence that *Sema3A* and *Sema3F* regulate the migration of GABAergic neurons in the developing neocortex. J. Comp. Neurol. **455:**238–248.
44. **Tamamaki, N., K. Nakamura, and T. Kaneko.** 2001. Cell migration from the corticostriatal angle to the basal telencephalon in rat embryos. Neuroreport **12:**775–780.
45. **Tanaka, D., Y. Nakaya, Y. Yanagawa, K. Obata, and F. Murakami.** 2003. Multimodal tangential migration of neocortical GABAergic neurons independent of GPI-anchored proteins. Development **130:**5803–5813.
46. **Taniguchi, H., D. Kawauchi, K. Nishida, and F. Murakami.** 2006. Classic cadherins regulate tangential migration of precerebellar neurons in the caudal hindbrain. Development **133:**1923–1931.
47. **Tissir, F., I. Bar, Y. Jossin, O. De Backer, and A. M. Goffinet.** 2005. Protocadherin *Celsr3* is crucial in axonal tract development. Nat. Neurosci. **8:**451–457.
48. **Tissir, F., O. De-Backer, A. M. Goffinet, and C. Lambert de Rouvroit.** 2002. Developmental expression profiles of *Celsr* (*Flamingo*) genes in the mouse. Mech. Dev. **112:**157–160.
49. **Tissir, F., and A. M. Goffinet.** 2006. Expression of planar cell polarity genes during development of the mouse CNS. Eur. J. Neurosci. **23:**597–607.
50. **Tuttle, R., Y. Nakagawa, J. E. Johnson, and D. D. O'Leary.** 1999. Defects in thalamocortical axon pathfinding correlate with altered cell domains in *Mash-1*-deficient mice. Development **126:**1903–1916.
51. **Usui, T., Y. Shima, Y. Shimada, S. Hirano, R. W. Burgess, T. L. Schwarz, M. Takeichi, and T. Uemura.** 1999. *Flamingo*, a seven-pass transmembrane cadherin, regulates planar cell polarity under the control of *Frizzled*. Cell **98:**585–595.
52. **Valcanis, H., and S. S. Tan.** 2003. Layer specification of transplanted interneurons in developing mouse neocortex. J. Neurosci. **23:**5113–5122.
53. **Waclaw, R. R., Z. J. Allen II, S. M. Bell, F. Erdélyi, G. Szabó, S. S. Potter, and K. Campbell.** 2006. The zinc finger transcription factor *Sp8* regulates the generation and diversity of olfactory bulb interneurons. Neuron **49:**503–516.
54. **Wada, H., H. Tanaka, S. Nakayama, M. Iwasaki, and H. Okamoto.** 2006. *Frizzled3a* and *Celsr2* function in the neuroepithelium to regulate migration of facial motor neurons in the developing zebrafish hindbrain. Development **133:**4749–4759.
55. **Wang, X., J. A. Weiner, S. Levi, A. M. Craig, A. Bradley, and J. R. Sanes.**

2002. Gamma protocadherins are required for survival of spinal interneurons. Neuron **36:**843–854.
56. **Wichterle, H., J. M. Garcia-Verdugo, D. G. Herrera, and A. Alvarez-Buylla.** 1999. Young neurons from medial ganglionic eminence disperse in adult and embryonic brain. Nat. Neurosci. **2:**461–466.
57. **Wichterle, H., D. H. Turnbull, S. Nery, G. Fishell, and A. Alvarez-Buylla.** 2001. In utero fate mapping reveals distinct migratory pathways and fates of neurons born in the mammalian basal forebrain. Development **128:**3759–3771.
58. **Wonders, C. P., and S. A. Anderson.** 2006. The origin and specification of cortical interneurons. Nat. Rev. Neurosci. **7:**687–696.
59. **Wonders, C. P., L. Taylor, J. Welagen, I. C. Mbata, J. Z. Xiang, and S. A. Anderson.** 2008. A spatial bias for the origins of interneuron subgroups within the medial ganglionic eminence. Dev. Biol. **314:**127–136.
60. **Wu, Q., and T. Maniatis.** 2000. Large exons encoding multiple ectodomains are a characteristic feature of protocadherin genes. Proc. Natl. Acad. Sci. USA **97:**3124–3129.
61. **Wu, Q., and T. Maniatis.** 1999. A striking organization of a large family of human neural cadherin-like cell adhesion genes. Cell **97:**779–790.
62. **Wu, S., G. Ying, Q. Wu, and M. R. Capecchi.** 2008. A protocol for constructing gene targeting vectors: generating knockout mice for the cadherin family and beyond. Nat. Protoc. **3:**1056–1076.
63. **Xu, Q., I. Cobos, E. De La Cruz, J. L. Rubenstein, and S. A. Anderson.** 2004. Origins of cortical interneuron subtypes. J. Neurosci. **24:**2612–2622.
64. **Yagi, T., and M. Takeichi.** 2000. Cadherin superfamily genes: functions, genomic organization, and neurologic diversity. Genes Dev. **14:**1169–1180.
65. **Zhou, L., I. Bar, Y. Achouri, K. Campbell, O. De Backer, J. M. Hebert, K. Jones, N. Kessaris, C. L. de Rouvroit, D. O'Leary, W. D. Richardson, A. M. Goffinet, and F. Tissir.** 2008. Early forebrain wiring: genetic dissection using conditional *Celsr3* mutant mice. Science **320:**946–949.
66. **Zou, C., W. Huang, G. Ying, and Q. Wu.** 2007. Sequence analysis and expression mapping of the rat clustered protocadherin gene repertoires. Neuroscience **144:**579–603.